Chapter 5

Photosynthesis

Photosynthesis is the physico-chemical process by which plants, algae and photosynthetic bacteria transduce light energy into chemical energy. In plants, algae and cyanobacteria, the photosynthetic process results in the release of molecular oxygen and the removal of carbon dioxide from the atmosphere which is used to synthesize carbohydrates (oxygenic photosynthesis). Purple bacteria (*Thiorhodaceae, Athiorhodaceae*), green sulfur bacteria (*Chlorobiacea*), green gliding bacteria (*Chloroflexaceae*), and Heliobacteria (photosynthesizing *Firmicutes*) use light energy to create organic compounds, but do not produce oxygen (anoxygenic photosynthesis). In all these cases light energy is absorbed by chlorophyll molecules and finally used to produce a transmembrane pH gradient. This pH gradient drives the synthesis of ATP, the universal energy provides in the living cell.

Beside these photosynthetic organisms, an additional taxonomic group, the so-called Halobacteria (*Halobacteriales*), exists that uses light energy directly to produce a transmembrane pH gradient and synthesize finally also ATP. A retinal molecule is involved in the light absorption and the generation of the pH gradient. The retinal changes its conformation in the excited state. A proton transfer across the membrane is coupled to the conformational transition. Halobacteria are, however, not able to use carbon dioxide as sole carbon source. Since the photosynthetic mechanism of these bacteria is fundamentally different to the oxygenic photosynthesis or anoxygenic photosynthesis, I do not describe its mechanism in the following.

Photosynthesis provides the energy to reduce carbon required for the survival of virtually all living systems on our planet. It creates molecular oxygen necessary for the survival of oxygen consuming organisms. The overall equation for photosynthesis is deceptively simple (eq 5.1).

$$6\ CO_2 + 6\ H_2O + h\nu \longrightarrow C_6H_{12}O_6 + 6\ O_2 \tag{5.1}$$

However, a complex set of physical and chemical reactions must occur in a coordinated manner for the synthesis of carbohydrates. To produce a sugar molecule such as sucrose, plants require many distinct proteins that work together within a complicated membrane structure. Photosynthesis is a special challenge in understanding several interrelated molecular processes that are partially coupled to membranes.

5.1 General Overview

Oxygenic and anoxygenic photosynthesis share many features. Photosynthesis in plants and algae takes place in specialized organelles, the chloroplasts. Also the photosynthetic protein

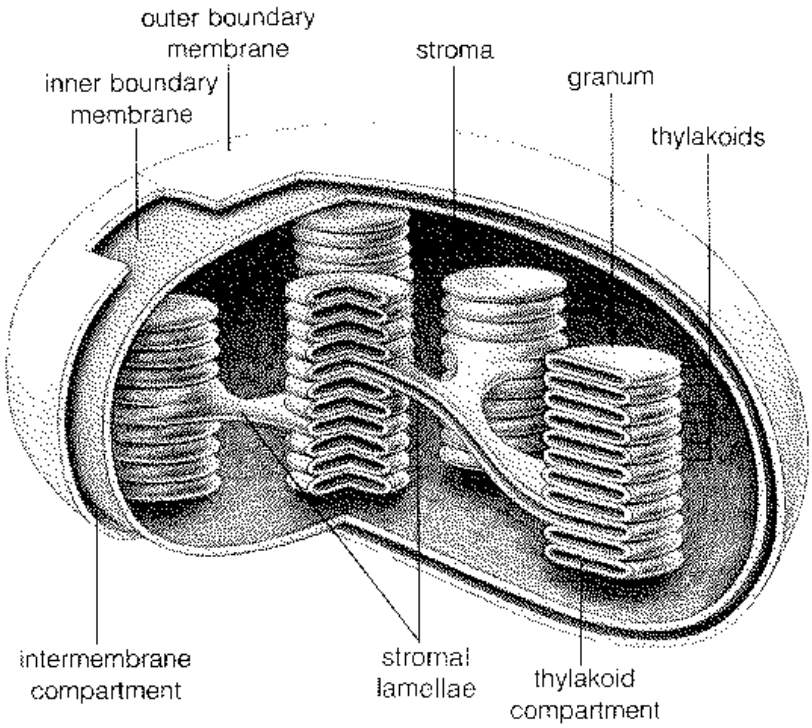

Figure 5.1: Schematical representation of a chloroplast. Chloroplasts are semi-autonomous organelles in plant cells. Light energy is transduced into chemical energy at the thylakoid membrane. Fixation of CO_2 takes place in the stroma.

complexes of bacteria are located in special membrane regions. Photosynthesis can be divided in two types of reactions, the light reactions and the dark reactions. In the light reactions, light energy is used to excite a cofactor. Then, an electron is transferred from there to its final acceptor. The excitation and the initial charge separation takes place in reaction centers. The reaction centers of all photosynthetic organisms are similar but differ to some extend in composition and in the redox potentials of the cofactors. Anoxygenic photosynthesis involves only one reaction center, while oxygenic photosynthesis involves two reaction centers. The reaction centers and a membrane-bound cytochrome complex of *bc*-type generate a transmembrane pH gradient. The ATP-synthase uses this pH gradient to produce ATP from ADP and inorganic phosphate. Furthermore, the light energy is used to reduce $NADP^+$ to NADPH. The ATP and NADPH produced in the light reactions drive the carbohydrate synthesis in the dark reactions. Carbohydrate synthesis is accomplished by the Calvin cycle, which is a complicated network of biochemical reactions. Also various regulatory processes couple the light and the dark reactions. In the following, I describe the molecular apparatus and the reactions involved in oxygenic photosynthesis.

5.1.1 Chloroplast Structure

Chloroplasts (Figure 5.1) are semi-autonomous organelles of plant cells. In most higher plants, they have the shape of a circular or elongated lens and a diameter of approximately 3–10μm. Chloroplasts consist of the outer and inner boundary membrane, a plasmatic matrix (stroma), and an internal membrane system (thylakoid). Like mitochondria, chloroplasts contain cyclic DNA and ribosomes similar to those of prokaryotes. There exist evidence that during early

evolution cyanobacteria entered the cell of archaic eukaryotes as endosymbionts (Voet & Voet, 1995; Kleinig & Sitte, 1986). These endosymbionts lost there independence during evolution. Proteins of recent chloroplast are partially encoded in the chloroplast genome and partially in the nuclear genome. A complicated protein translocation machinery maintains the targeting of the polypeptides encoded in the nuclear genome to chloroplasts (Schatz & Dobberstein, 1996). Several recent articles review structural and functional aspects of chloroplasts (Staehelin, 1986; Staehelin & van der Staay, 1996).

The lipid composition of the outer boundary membrane is similar to that of eukaryotic cell membranes while the lipid composition of the inner boundary membrane is similar to that of prokaryotes (Kleinig & Sitte, 1986). The boundary membranes are involved in the transport of photosynthetic metabolites, in protein translocation, in lipid transfer, and in the exchange of ions. Most of the proteins that are actively involved in the transfer processes are located in the inner boundary membrane. The outer boundary membrane serves primarily as a physical barrier for large molecules such as proteins and nucleic acids.

The chloroplast stroma is the plasmatic compartment between the inner boundary membrane and the thylakoid membrane. It contains enzymes of the Calvin cycle (especially the enzyme ribulose bisphosphat carboxylase), multiple copies of the circular DNA and all components of the transcription and translation machinery, and enzymes for the synthesis of lipids, porphyrins, terpenoids, quinoids and other aromatic compounds. Besides, starch granules and lipidic globuli can accumulate.

All light absorption and energy-transducing processes take place at the thylakoid membranes. The thylakoid membranes enclose a so-called thylakoid compartment or thylakoid space. All parts of the thylakoid space are presumably interconnected. The thylakoid network comprises two different membranes; a cylindrical stack of appressed thylakoids (grana) and single layered thylakoid membranes joining the grana regions (stroma thylakoids). The pH difference between the thylakoid space and the stroma is about 2 to 3. If only the protons would maintain the membrane potential, the potential difference would be about 120 mV to 180 mV according to Nernst equation. The measured membrane potential is however only 10 mV due to the contribution of additional ions (Vredenberg, 1997). Thylakoid membranes contain ion channels besides proteins that are directly involved in the energy transduction processes, (Schönknecht *et al.*, 1995; Pottosin & Schönknecht, 1996). These ion channels lower the membrane potential and thus the energy required to transfer a proton across the membrane. The lipid composition of thylakoid membranes differs from that of other plant membranes. Besides lipids that are unique to thylakoid membranes, it contains polyunsaturated fatty acids to an exceptional large amount, which makes the thylakoid membranes highly fluid allowing a rapid diffusion of membrane protein complexes.

The membrane proteins involved in the light reactions of photosynthesis are not equally distributed over the thylakoid membrane. Photosystem II and the light harvesting complex II concentrate in the grana thylakoids, while photosystem I and the ATP-synthase concentrate in the stroma thylakoids. The cytochrome b_6f complex has nearly the same concentration in both thylakoid regions. The functional reason for the grana stacking is presumably to maintain the separation of photosystem II and photosystem I. Without physical separation of the two photosystems, photosystem I would unbalance the excitation energy within the pigment bed of photosystem II. Furthermore, photosystem I is more efficient in exciton usage (Staehelin & van der Staay, 1996).

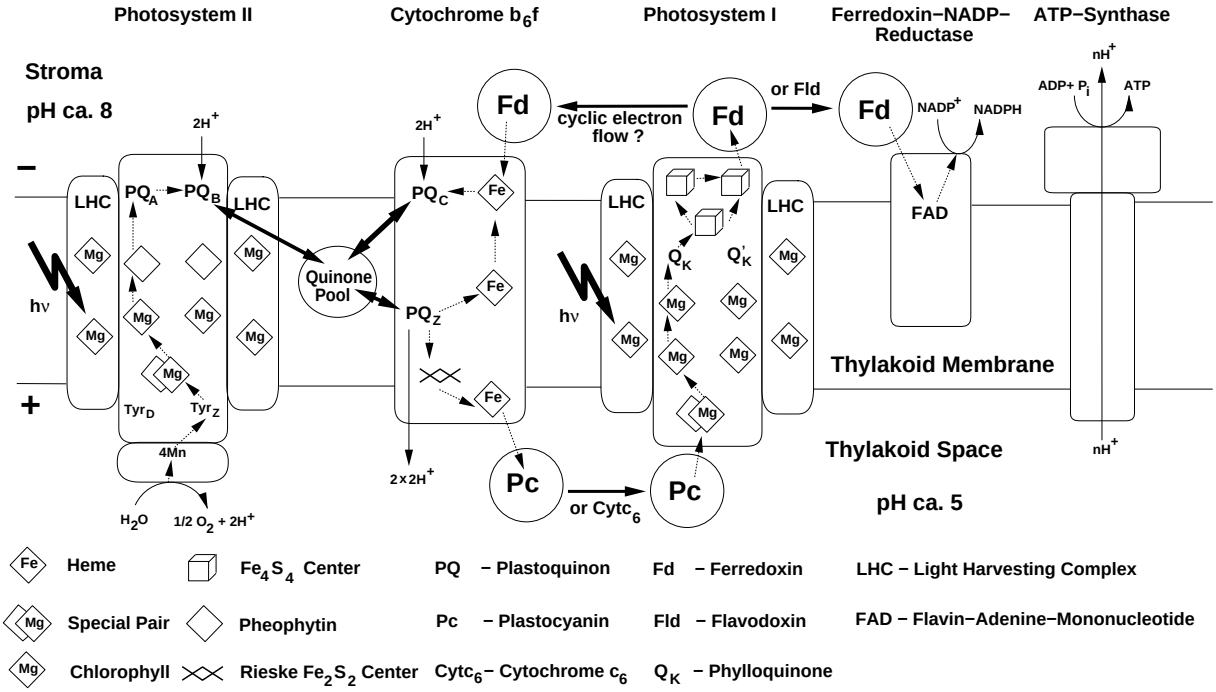

Figure 5.2: Light reactions of oxygenic photosynthesis. Electron and proton transfer involves four membrane-spanning proteins (photosystem II, cytochrome b_6f, photosystem I, ATP-Synthase), one protein that is associated to the membrane (Ferredoxin-NADP-Reductase) and two soluble proteins (plastocyanin, ferredoxin). ATP-synthase uses the pH gradient to form an ATP from ADP and inorganic phosphate. The general pathway of the electron flow from the primary donor (water) to the final acceptor (NADPH) is known in detail, while much less is known about the cyclic electron flow. It is not clear whether ferredoxin interacts with cytochrome b_6f or not. Dotted lines, thin solid lines, and thick solid lines indicate electron-transfer reactions, proton transfer reactions, and diffusion processes respectively.

5.1.2 The Light Reactions

The light reactions of photosynthesis convert light energy into a transmembrane pH gradient, i. e., into electrochemical energy. The ATP-synthase uses the pH gradient to form an ATP from ADP and inorganic phosphate and thus converts the electrochemical into chemical energy. Figure 5.2 shows a schematic representation of the energy transducing reactions involved in the light reactions of photosynthesis. In the last couple of years, a tremendous amount of structural information of proteins involved in the light reactions of photosynthesis became available. With the aid of these structures, experimentalists and theoreticians can gain insight in structure-function relationships of these proteins and the photosynthetic process as a whole. Photosynthesis might be one of the first complex biochemical reactions coupled to membranes for which a detailed structural and functional picture can be drawn.

Light harvesting complexes absorb light energy and transfer the excitation energy to the special pair, a chlorophyll dimer. In photosystem II, the excited special pair releases one electron. This electron is transferred via chlorophyll, pheophytin, and quinone (Q_I or Q_A) to a quinone acceptor (Q_{II} or Q_B). After the quinone received two electrons and two protons, it leaves its binding pocket and enters the membrane. The oxidized special pair oxidizes a tyrosine, Tyr_Z, close the water-oxidizing manganese cluster. In a multiple step reaction (Yachandra

et al., 1996), which is not completely understood, the manganese cluster get oxidized by Tyr_Z and the manganese cluster oxidizes water which lead to the release of molecular oxygen and four protons. At least four photons are required to oxidize one water and to release two quinoles from the Q_B site. The structure of light harvesting complexes were resolved recently (for review see Kühlbrandt, 1994; Fufe & Cogdell, 1994; Pullerits & Sundström, 1996). The structure of the purple bacterial photosynthetic reaction center was the first membrane protein resolved in great detail (Deisenhofer *et al.*, 1985). The purple bacterial photosynthetic reaction center shows many similarities to the core complex of photosystem II and was therefore often used as model for photosystem II. Recently, the structure of the core complex of photosystem II was determined by electron microscopy (Rhee *et al.*, 1997).

The quinone released from photosystem II enters the so-called Q-cycle. The Q-cycle is a reaction cycle performed by cytochrome b_6f that couples electron transfer to proton transfer. Several models for the reaction sequences exist (Cramer & Knaff, 1991). A similar Q-cycle exists in the mitochondrial electron-transfer chain (Brandt & Trumpower, 1994; Brandt, 1996). The function of cytochrome b_6f is to increase the transmembrane pH gradient. Cytochrome b_6f contains two *b*-type cytochromes, one Rieske iron-sulfur cluster, and one *c*-type cytochrome (cytochrome f) (for review see Cramer *et al.*, 1994a; Cramer *et al.*, 1994b; Cramer *et al.*, 1996; Kallas, 1993). Besides, cytochrome b_6f contains a chlorophyll *a* molecule of unknown function (Pierre *et al.*, 1997). Cytochrome b_6f has two plastoquinone binding sites, PQ_C and PQ_Z. The plastoquinone at PQ_Z reduces cytochrome f via the Rieske protein. Protons are released upon this reaction to the thylakoid space. The structure of the luminal domains of cytochrome f (Martinez *et al.*, 1994; Martinez *et al.*, 1996) and of the Rieske protein (Carrell *et al.*, 1997) have been determined at atomic resolution. A two-dimensional projection map of cytochrome b_6f at 8 Å resolution is also available (Pierre *et al.*, 1997). Recently the structure of several cytochrome bc_1 complexes, the mitochondrial analogue of cytochrome b_6f, was resolved by x-ray crystallography (Xia *et al.*, 1997; Zhang *et al.*, 1998).

Plastocyanin is a small water-soluble blue-copper protein, which transfers electrons from cytochrome b_6f to photosystem I in the thylakoid space. Under conditions of copper deficiency, cytochrome c_6 replaces plastocyanin in cyanobacteria and some algae. The structures of cytochrome c_6 and plastocyanin were determined at great detail by x-ray crystallography and NMR spectroscopy (for review see Redinbo *et al.*, 1994; Navarro *et al.*, 1997). The interaction of cytochrome c_6 and plastocyanin with cytochrome f and photosystem I is also intensively investigated (Navarro *et al.*, 1997). We performed a theoretical study on the docking of plastocyanin and cytochrome f (Ullmann *et al.*, 1997b). Subsequently, Ubbink *et al.*, 1998 performed a NMR analysis of the plastocyanin-cytochrome f complex and obtained a structural model based on their experimental data that is very similar to one model we proposed previously.

Photosystem I is the third membrane-bound electron-transfer protein taking part in the light reactions of photosynthesis. The core complex contains one chlorophyll dimer, four chlorophyll molecules, two quinones, and three Fe_4S_4 clusters. Besides, these cofactors about one hundred chlorophyll molecules surround the core complex and function as light harvesting molecules. After excitation of the P700 (the special pair) to $P700^*$, an electron is transferred in a multiple step reaction form $P700^*$ to one of the three iron-sulfur clusters. The iron-sulfur cluster reduces ferredoxin which docks to photosystem I at the stroma side. $P700^+$ is reduced by plastocyanin. A low resolution structure of photosystem I (4 Å) was determined recently (Krauss *et al.*, 1993; Krauss *et al.*, 1996; Schubert *et al.*, 1997). Also electron microscopic investigations on photosystem I were performed (Karrasch *et al.*, 1996).

Ferredoxin is a soluble Fe_2S_2 iron-sulfur protein in the stroma of chloroplasts. It transfers electrons from photosystem I to ferredoxin-$NADP^+$ reductase. Besides, ferredoxin reduces several other proteins such as ferredoxin-thioredoxin reductase, glutamate synthase, and nitrate reductase (Knaff & Hirasawa, 1991). The structure of ferredoxin was determined for several species by NMR and crystallographic techniques (Smith *et al.*, 1983, Tsukihara *et al.*, 1990, Rypniewski *et al.*, 1991, Fukuyama *et al.*, 1995, Baumann *et al.*, 1996, Hatanaka *et al.*, 1997). Under conditions of iron deficiency, ferredoxin is replaced by the flavin-mononucleotide-phosphate containing protein flavodoxin for which the structure is also known at great detail (Rao *et al.*, 1993, Fukuyama *et al.*, 1990). Ferredoxin influences the dark reactions of photosynthesis by activating or deactivating the enzymes fructose-bisphosphatase and seduheptulose-bisphosphatase via ferredoxin-thioredoxin reductase and thioredoxin.

Ferredoxin-NADP reductase is a flavin-adenine dinucleotide containing protein. It is associated to the stromal side of the thylakoid membrane. The protein which mediates the membrane association is not unequivocally known. Probably subunit E of photosystem I is involved in the membrane association of ferredoxin-NADP reductase(Andersen *et al.*, 1992). Ferredoxin-$NADP^+$ reductase oxidizes two ferredoxins and uses the electrons to reduce $NADP^+$ to NADPH, which is needed in the dark reactions of photosynthesis. The crystal structure of ferredoxin-$NADP^+$ reductase is known with and without $NADP^+$ associated to the protein (Karplus *et al.*, 1991; Serre *et al.*, 1996).

The ATP-synthase uses the pH gradient generated by photosystem II and cytochrome b_6f to synthesize ATP from ADP and inorganic phosphate. The protein is subdivided into two regions, the membrane spanning part F_o and the stromal part F_1. The stromal part F_1 rotates in a 120^o interval and synthesizes ATP in three steps (for review see Nakamoto, 1996; Fillingame, 1996; Junge, 1997). The structure of F_1 of the closely related mitochondrial ATP-synthase was resolved recently (Abrahams *et al.*, 1998). The ATP obtained from this reaction is used in the dark reactions of photosynthesis to synthesize carbohydrates.

Because the two photosystems work together in oxygenic photosynthesis, water can be used as primar electron donor for carbon fixation. Beside the electron transfer from water to NADPH, also a cyclic electron transfer occurs in the chloroplasts (Bendall & Manasse, 1995). Much less is, however, known about cyclic electron transfer. Cyclic electron transfer involves photosystem I, cytochrome b_6f, plastocyanin, plastoquinones, ferredoxin, and probably also ferredoxin-$NADP^+$ reductase. About the presence of an additional enzyme called ferredoxin-plastoquinone reductase was speculated; such activities may however be also intrinsically be performed by other components of the thylakoid membrane such as photosystem I or ferredoxin-$NADP^+$ reductase (Bendall & Manasse, 1995).

5.1.3 The Dark Reactions

The light energy is converted into the chemical energy of ATP during the light reactions of photosynthesis. It is, however, very inefficient to store the energy in the form of ATP and NADPH. Carbohydrates or lipids need much less volume to save the same amount of energy. During the dark reactions of photosynthesis, the chemical energy of ATP is interconverted into the chemical energy of carbohydrates. Furthermore this energy is used to fix carbodioxide in the Calvin cycle. Plants and cyanobacteria are therefore able to use carbodioxide as sole carbon source. The enzymes of the Calvin cycle are located in the stroma of the chloroplasts. Although, none of the dark reactions of photosynthesis was investigated in this work, I briefly summarize the main features of the Calvin cycle for the sake of completeness.

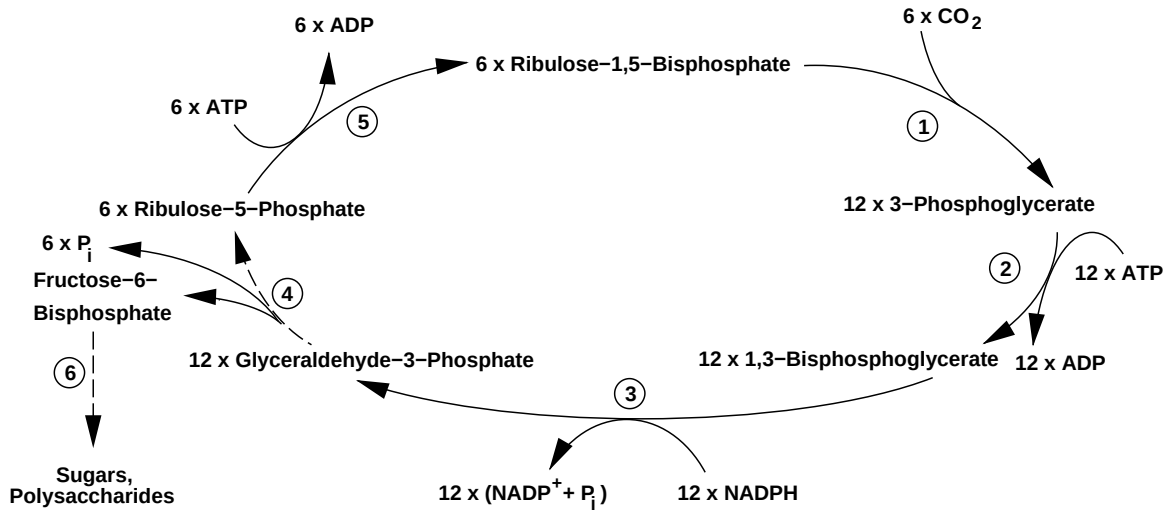

Figure 5.3: Calvin Cycle. 1) Ribulose-1,5-bisphosphate carboxylase cleaves ribulose-1,5-bisphosphate and attaches a CO_2 to one of the fragments. Two 3-phosphoglycerate molecules emerge out of one ribulose-1,5-bisphosphate and one CO_2. 2) Phosphoglycerate kinase phosphorylates 3-phosphoglycerate to 1,3-bisphosphoglycerate. 3) Glyceraldehyde-3-phosphate dehydrogenase reduces the phosphorylated carboxyl group to an aldehyde group. 4) The resulting glyceraldehyde-3-phosphate is used for the synthesis of fructose-6-phosphate, the product of the Calvin cycle. Ribulose-5-phosphate is regenerated from glyceraldehyde-3-phosphate in a complex reaction scheme which involves several enzymes. 5) Ribulose-5-phosphate is phosphorylated to ribulose-1,5-bisphosphate carboxylase by the enzyme phospho-ribulose kinase. This reaction closes the Cavin cycle. 6) The product fructose-6-phosphate is used to synthesize sugars and polysaccharides such as starch and cellulose.

The Calvin cycle can be divided in two stages. In the first stage ATP and NADPH is used to fix carbodioxide. Two NADPH molecules and three ATP molecules are required to fix one carbodioxide molecule. In the second stage, the carbon atoms are shuffled to enable the release of one sugar molecule. The sugar is then used to synthesize other molecules or stored in the form of polysaccharides such as starch or cellulose. The major steps of the first stage of the Calvin cycle are summarized in Figure 5.3. The key enzyme of the Calvin cycle is ribulose-bisphosphate carboxylase (Cleland *et al.*, 1998).

5.2 Coupling of Electron-Transfer and Protonation Reactions in the Bacterial Photosynthetic Reaction Center

The bacterial photosynthetic reaction center (bRC) is a pigment-protein complex in the membrane of purple bacteria. It converts light energy into electrochemical energy by coupling photo-induced electron transfer to proton uptake from cytoplasm. The crystal structure of the bRC from *Rhodopseudomonas (Rps.) viridis* (Deisenhofer *et al.*, 1985; Deisenhofer *et al.*, 1995; Lancaster & Michel, 1996) and from *Rhodobacter (Rb.) sphaeroides* (Allen *et al.*, 1987; Ermler *et al.*, 1994) enabled a more detailed understanding of the various functional processes in the bRC. Four polypeptides form the bRC from *Rps. viridis*: the L, H, and M subunits and a tightly-bound four-center *c*-type cytochrome. These polypeptides bind fourteen cofactors: one carotenoid, four hemes, four bacteriochlorophylls, two bacteriopheophytins, one menaquinone, one ubiquinone, and one non-heme iron. The chlorophylls, the pheophytins, and the quinones

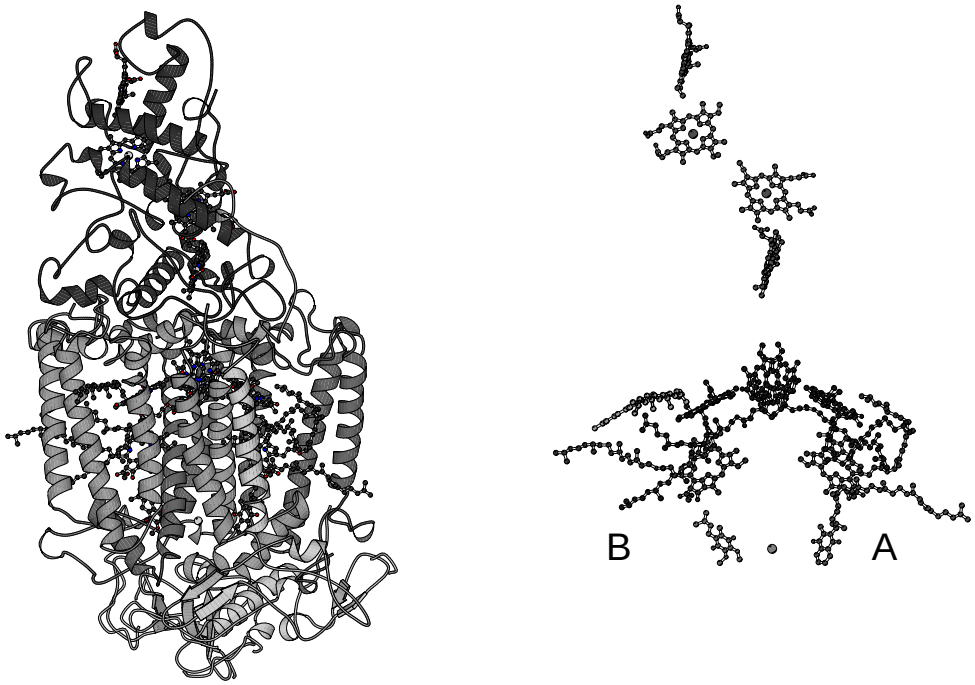

Figure 5.4: Bacterial Photosynthetic Reaction Center. Left: The polypeptides with the embedded cofactors. Right: Only the cofactors are shown. From th top to the bottom: four hemes, four bacteriochlorophylls, two pheophytins, one neurosporin, one menaquinone and one ubiquinone, and oner iron.

arrange in two branches, A and B, related by a approximate C_2 symmetry and extend from the special pair to the quinones (see Figure 5.4). Only branch A, is electron-transfer active. Its cofactors are predominantly embedded in the L subunit. Electronic excitation of the special pair, a bacteriochlorophyll dimer, induces a multi-step electron transfer from the special pair to Q_A, which is a menaquinone in the bRC from *Rps. viridis*. From there the electron moves to the Q_B, which is a ubiquinone. After this initial reaction, a second electron transfer from Q_A to Q_B and two protonation reactions of Q_B follow, resulting in a dihydroquinone Q_BH_2. The dihydroquinone leaves its binding site and is replaced by an oxidized ubiquinone from the quinone pool. The temporal order of these reactions is, however, not completely resolved (for a review see Okamura & Feher, 1992). Recently, Graige *et al.*, 1996 proposed several models for the coupling of the protonation of Q_B to the electron transfer between Q_A and Q_B. Based on their kinetic data, they favored either a mechanism in which the second electron transfer to Q_B occurs in a concerted manner with the first protonation of Q_B or a mechanism in which the first protonation of Q_B precedes the second electron transfer. The dihydroquinone Q_BH_2 has two acidic protons, one at the quinone oxygen atom proximate to the non-heme iron (near His L190), the other at the quinone oxygen atom distant from the non-heme iron (near Ser L223). Thus, there are two possibilities for the first protonation of Q_B.

5.2.1 Total Protonation and Protonation Patterns

Proton uptake by wild type and mutant bRC's during electron-transfer and protonation reactions of the quinones were studied experimentally by several research groups (Maróti & Wraight, 1988; McPherson *et al.*, 1988; McPherson *et al.*, 1993; Sebban *et al.*, 1995). However, these

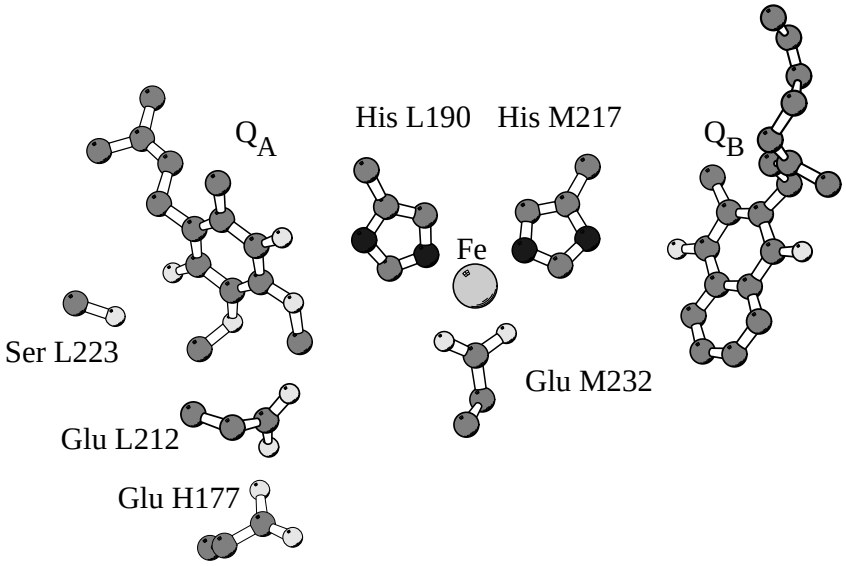

Figure 5.5: Structural arrangement of the quinone binding pockets. View of the two quinones, the non-heme iron with ligands (His-L230 and His-M264 are omitted for the sake of clarity), and nearby putatively functional residues. Glu-L212 is almost completely protonated in all states at pH 7.5. At Glu-H177 most of total protonation changes are localized. Ser-L223 is important for the first proton transfer. The oxygen atom of Q_B pointing towards and away from the non-heme iron are called proximal and distal oxygen atom, respectively.

investigations were done at the bRC from *Rb. sphaeroides* (Maróti & Wraight, 1988; McPherson *et al.*, 1988; McPherson *et al.*, 1993) and from *Rb. capsulatus* (Sebban *et al.*, 1995) but not from *Rps. viridis*. Much effort was spent to assign changes in total protonation to specific residues. One of the titratable groups in proximity to Q_B is Glu L212 (closest atom pair distance 3 Å, Figure 5.5). Mutation studies indicate a pK_a-value of Glu L212 of 9.0 to 9.5 (Paddock *et al.*, 1989; Takahashi & Wraight, 1992) and imply no participation of Glu L212 in proton uptake at pH 7.5 and below (McPherson *et al.*, 1994; Miksovska *et al.*, 1996). However, time resolved IR measurements suggest a protonation of Glu L212 after formation of $Q_B^{\cdot-}$ (Hienerwadel *et al.*, 1995). The latter observation is supported by electrostatic calculations at the bRC from *Rb. sphaeroides* (Beroza *et al.*, 1995) and from *Rps. viridis* (Lancaster *et al.*, 1996). In both theoretical studies, it is proposed that the protonation of Glu L212 contributes to a significant part to the total proton uptake by the bRC associated with $Q_B^{\cdot-}$ formation.

Using a continuum electrostatic method, we calculated the protonation patterns and the total protonation of the bRC for all possible states of the quinones as shown in Figure 5.6. In contrast to previous theoretical studies by other groups (Beroza *et al.*, 1995; Lancaster *et al.*, 1996), we considered not only those bRC states in which the quinones are in different redox states, but also those bRC states in which Q_B is protonated. Table 5.1 shows the protonation probability of non-standard protonated residues that are less than 25 Å away from the quinones. Furthermore, the difference between the total protonation of the ground state Q_AQ_B of the bRC and the total protonation of the respective other states are listed in comparison to experimental values. Our results imply that the proton uptake by the bRC occurs predominantly during the redox reactions of the quinones, whereas the proton uptake by the bRC coupled to the protonation of Q_B is smaller. The uptake of about 0.2 protons on average goes along with

Table 5.1: Total protonation and some single-site protonations at pH 7.5. All residues within a distance of 25 Å from the quinones and with at least 0.05 protons deviation from standard protonation are shown, except N-termini of L- and M-chain which are completely deprotonated in all states. Histidines protonated only at $N_{\varepsilon 2}$ are considered to be in standard protonation and are therefore not included in the table.

state	histidine (tautomers)[1]				glutamate					total[2]	
of	L211		M16		H45	H177	H234	L104	L212	this	experimental
quinones	δ	ε	δ	ε						calculation	values
Q_AQ_B	0.47	0.53	0.25	0.73	0.05	0.03	0.27	1.00	0.99	0.00	0.00
$Q_A^{\cdot-}Q_B$	0.50	0.50	0.25	0.72	0.06	0.06	0.30	1.00	0.99	0.14	0.24[3]/ 0.34[4,5]
$Q_AQ_B^{\cdot-}$	0.53	0.47	0.25	0.73	0.05	0.59	0.26	1.00	1.00	0.60	0.37[5]/ 0.90[4]
$Q_A^{\cdot-}Q_B^{\cdot-}$	0.53	0.47	0.25	0.73	0.06	0.80	0.27	1.00	1.00	0.88	
$Q_A^{\cdot-}Q_BH_{dist}$	0.48	0.52	0.25	0.73	0.06	0.05	0.31	1.00	1.00	1.15	
$Q_A^{\cdot-}Q_BH_{prox}$	0.48	0.52	0.25	0.73	0.06	0.07	0.30	1.00	0.98	1.14	
$Q_AQ_B^{2-}$	0.58	0.42	0.24	0.74	0.05	0.99	0.25	1.00	1.00	0.97	
$Q_AQ_BH_{dist}^-$	0.54	0.46	0.25	0.73	0.05	0.68	0.25	1.00	1.00	1.68	1.3[7]
$Q_AQ_BH_{prox}^-$	0.52	0.48	0.24	0.74	0.05	0.65	0.25	1.00	1.00	1.65	
$Q_AQ_BH_2$	0.46	0.54	0.24	0.73	0.05	0.03	0.28	1.00	0.99	2.01	1.9[6]/ 2.1[7]

[1] remaining part is protonated at $N_{\delta 1}$ and $N_{\varepsilon 2}$
[2] expressed as difference to the ground state
[3] *Rb. capsulatus* (Sebban *et al.*, 1995)
[4] *Rb. sphaeroides* (Maróti & Wraight, 1988)
[5] *Rb. sphaeroides* (McPherson *et al.*, 1988)
[6] *Rb. sphaeroides* (McPherson *et al.*, 1993)
[7] *Rb. sphaeroides* (Glu-L212→Gln mutant, McPherson *et al.*, 1994)

each of the two reduction steps of Q_A (Figure 5.6). With exception of the electron transfer to the singly-reduced, unprotonated Q_B, all electron transfers from Q_A to Q_B are coupled to an uptake of about 0.5 protons on average (Figure 5.6). The protonation of Q_B in the states $Q_A^{\cdot-}Q_B^{\cdot-}$, $Q_A^{\cdot-}Q_BH_{dist}$, and $Q_A^{\cdot-}Q_BH_{prox}$ induces an uptake of about 0.3 protons on average only (Figure 5.6). This means that an excess proton is already partially available in the protein matrix, before the protonation of Q_B actually occurs.

Our calculated changes of the total protonation are in reasonable agreement with the experimental results. However, the measured value of proton uptake depends sensitively on details of the experimental procedure, so that different groups got significantly different results (Table 5.1). Discrepancies between experiments and calculations may be explained by the following arguments. (I) Most experimental values are obtained from bRC's of purple bacteria other than *Rps. viridis*, which is explored in this study. (II) Experimental values can not easily be assigned to a specific bRC state, since often only the redox state and not the protonation state of the quinones is determined by experimental conditions. We assigned the experimental values of protonation changes to the states that are, according to our calculated energies (see below), occupied with the highest probability. In addition, experimental values from different groups vary. Some experiments indicate a coupling of the proton uptake by the protein matrix during the first electron transfer from Q_A to Q_B (Maróti & Wraight, 1988; Baciou *et al.*, 1991), others do not (McPherson *et al.*, 1988). Our calculations suggest also a coupling of the first electron transfer between Q_A and Q_B to proton uptake by the protein matrix (see Table 5.1) and thus imply a pH dependence of the reaction energies of this electron transfer.

Earlier electrostatic calculations by other groups tend to give higher values for total protonation differences with respect to the ground state Q_AQ_B than our calculations, especially for

the state $Q_A Q_B^{2-}$. The differences between our results and those obtained by Beroza *et al.*, 1995 may be related to the different bRC considered in the calculations. Beroza *et al.*, 1995 used the bRC from *Rb. sphaeroides* while Lancaster *et al.*, 1996 and we used the bRC from *Rps. viridis*. The bRC structures used by Lancaster *et al.*, 1996 and us are very similar, since we adjusted the structure of Deisenhofer *et al.*, 1995 according to the available information about the structure determined by Lancaster *et al.* (Lancaster & Michel, 1996; Lancaster *et al.*, 1995). Thus, the most probable source for the discrepancies between their and our results are the different atomic partial charges. We used atomic partial charges derived from quantum-chemical calculations, for which the charge difference between the different protonation and redox states is distributed over all atoms of the respective quinone. Lancaster *et al.*, 1996 used atomic partial charges, for which the charge difference between different quinone redox states is exclusively localized at the carbonyl carbon and carbonyl oxygen atoms of the quinone ring. This more localized charge difference may explain the larger effects of the quinone redox states on the total protonation of the bRC.

Several titratable groups contribute to the proton uptake by the whole bRC, but most of them participate only with very small protonation changes. Besides the Q_B, the residue Glu H177 has the largest contribution to the proton uptake (Table 5.1). The distance of the carboxyl oxygen atom of this residue to the distal oxygen atom of Q_B is 8.0 Å (Figure 5.5). Glu H177 is possibly also involved in the proton transfer pathway from the solvent to Q_B (Lancaster *et al.*, 1995). According to our calculations, Glu L212 does not contribute significantly to the proton uptake at pH 7.5, since it is nearly protonated for all redox and protonation states of Q_A and Q_B. This result is not in agreement with previous calculations (Beroza *et al.*, 1995; Lancaster *et al.*, 1996), which suggest that Glu L212 is involved significantly in the proton uptake upon Q_B^- formation. However, the very small, but not vanishing ionization probability of Glu L212 of one to two percent in the states in which Q_B is neutral, shows that Glu L212 just starts to titrate at pH 7.5. The statistical uncertainty of the protonation probability of Glu L212 is less than 10^{-3} protons in our computation.

Our calculations support the above mentioned experimental results (Paddock *et al.*, 1989; Takahashi & Wraight, 1992; McPherson *et al.*, 1994; Miksovska *et al.*, 1996) that Glu L212 is not ionized at pH $<$7.5, but it is at least partially ionized and involved in proton uptake at pH $>$7.5 (McPherson *et al.*, 1994; Miksovska *et al.*, 1996). However, these results are obtained with the bRC from *Rb. sphaeroides* (Paddock *et al.*, 1989; Takahashi & Wraight, 1992; McPherson *et al.*, 1994) and from *Rb. capsulatus* (Miksovska *et al.*, 1996) but not from *Rps. viridis*, which was used for these calculations. Our results can not support the interpretation of the time-resolved IR measurements suggesting an involvement of Glu L212 in the proton uptake at pH 7.5 (Hienerwadel *et al.*, 1995). Also Hienerwadel *et al.*, 1995 discussed the uncertainty in assigning the observed spectroscopic effects to specific residues. According to our calculations, we would prefer an assignment to Glu H177. However, since Glu H177 and Glu L212 are strongly coupled (about 5 p*K*-units), small changes in the protein environment may cause that Glu L212 rather than Glu H177 changes its protonation during Q_B reduction. Regardless of this uncertainty, a mutation of Glu L212 will influence the protonation behavior of Glu H177, since the carboxyl carbon atoms of the two residues are only 6.8 Å apart.

5.2.2 Energetics of Electron Transfer and Protonation

Using a continuum electrostatic model, we calculated equilibrium constants for electron-transfer and protonation reactions of the quinones. From these equilibrium constants we obtained the

reaction energies. The calculated energy values are given in Figure 5.6 and will be discussed in the following sections.

First Electron Transfer from Q_A to Q_B

Measured equilibrium constants for the first electron transfer from Q_A to Q_B in the bRC from *Rps. viridis* are 900±50 at pH 6.0 and about 300 at pH 7.5 and 9.0 (Baciou *et al.*, 1991), which correspond to free energy changes of -175 meV and -150 meV, respectively. An earlier measurement gave an equilibrium constant of about 100 at pH 9.0 (Shopes & Wraight, 1985), which corresponds to a free energy change of -120 meV. Our continuum electrostatic calculations yielded an energy difference of -160 meV at pH 7.5. In the bRC from *Rb. sphaeroides* the measured reaction energy of the first electron transfer from Q_A to Q_B is about -70 meV (Kleinfeld *et al.*, 1984; Mancino *et al.*, 1984). Recent continuum electrostatic calculations at the bRC from *Rb. sphaeroides* were not able to reproduce this value. The energy was obtained with the wrong sign and was 230 meV higher than the experimental value (Beroza *et al.*, 1995). This may be due to problems with the crystal structure of the bRC from *Rb. sphaeroides* or due to the used atomic partial charges, which were not obtained from quantum-chemical computations.

In a recent crystallographic study, conformational differences between the dark-state structure (Q_AQ_B) and the light-state structure ($Q_AQ_B^{\cdot-}$) of the bRC from *Rb. sphaeroides* were described (Stowell *et al.*, 1997). The Q_B environment of the light structure in this study is very similar to most other available structures of the bRC, which are believed to represent the dark state, i. e., the Q_AQ_B state. However, one bRC structure from *Rb. sphaeroides* possesses a significantly different conformation at the Q_B binding site (Ermler *et al.*, 1994). Presumably, the Q_B in this structure is in the hydroquinone state (Lancaster & Michel, 1996). The putative hydroquinone-state structure (Ermler *et al.*, 1994) has very similar features at the Q_B site as the dark-state structure from Stowell *et al.*, 1997. In both structures, Q_B is rotated by about 180° and shifted outwards by about 5 Å compared to the other bRC structures, which are supposed to be in the dark state. These similarities are surprising. Hence it seems not to be clear, which conformational changes, if any, are important. In the present study, we did not consider conformational relaxation and fluctuation processes. In a more recent study, we used an iterative energy minimization scheme to calculate the redox potentials and the protonation energies for the various bRC states (Rabenstein *et al.*, 1998a). These energy minimizations, however, do not improve the present results.

Second Electron Transfer from Q_A to Q_B and first protonation of Q_B

Three different reactions may follow the first electron-transfer process: (I) the second electron transfer from Q_A to Q_B, (II) the protonation at the proximal oxygen of Q_B, i. e., the oxygen atom pointing towards the non-heme iron, or (III) the protonation at the distal oxygen of Q_B, i. e., the oxygen atom pointing away from the non-heme iron (Figure 5.6). Based on experimental results, different models were proposed. McPherson *et al.*, 1994 came to the conclusion that the first electron transfer is followed by the second electron transfer, whereupon the two protonations of Q_B occur. In contrast, the kinetic results of Graige *et al.*, 1996 fitted best to a model in which the first electron transfer is followed by the first protonation. Subsequently, the second electron transfer occurs as the rate determining step. Another model, fitting the kinetic results of Graige *et al.*, 1996 almost as good, includes a concerted mechanism, in which the second electron and the first proton are transferred to Q_B simultaneously. The model derived from

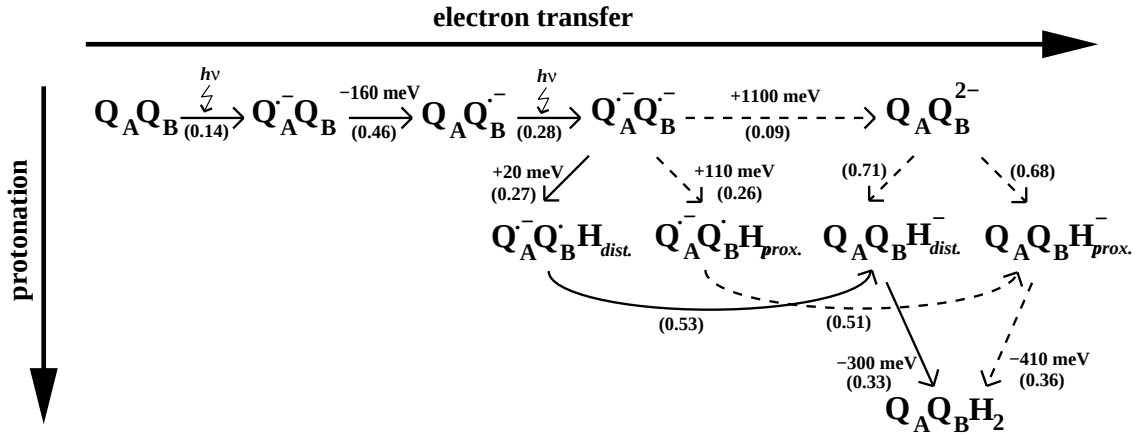

Figure 5.6: Scheme of the possible electron-transfer and protonation reactions involving the quinones of the bRC. Solid arrows are used for the energetically preferred reaction sequence. Calculated reaction energies are given near the respective arrows. Changes in total protonation during the reactions are given in parentheses.

mutation studies of Paddock *et al.*, 1990 supports also a reaction sequence in which the first electron transfer from Q_A to Q_B is followed by the first protonation of Q_B, the second electron transfer from Q_A to Q_B, and finally by the second protonation of Q_B. In addition, the model of Paddock *et al.*, 1990 proposes that the first protonation occurs at the distal oxygen atom of Q_B and the second proton binds to the proximal oxygen atom.

We calculated the reaction energy for the second electron transfer from Q_A to Q_B and also for the first protonation of Q_B at the distal and at the proximal oxygen atom (Figure 5.6). The energy difference between the bRC states $Q_A^{\cdot -}Q_B^{\cdot -}$ and $Q_AQ_B^{2-}$ is +1100 meV. This energy difference is even higher than the energy difference between the respective quinone states in aqueous solution (720 meV). Thus, according to our calculations, a doubly-reduced, unprotonated Q_B is unlikely to occur in the bRC. The protonation energy of Q_B in the bRC state $Q_A^{\cdot -}Q_B^{\cdot -}$ at pH 7.5 is also positive, but small (Figure 5.6). The protonation at the distal oxygen atom is energetically preferred by 90 meV. Therefore, we propose that after the first electron transfer from Q_A to Q_B, Q_B gets protonated at the distal oxygen atom. This is in agreement with the model of Paddock *et al.*, 1990. However, the difference between the protonation energies at the distal and proximal oxygen atom is small. If the protonation at the proximal oxygen is kinetically preferred it may precede the protonation of the distal oxygen atom.

The energy of +20 meV for the first protonation of Q_B at the distal oxygen atom corresponds to an equilibrium partial protonation of about 30 %. This fraction may be too small to detect the singly-protonated Q_B spectroscopically. However in the bRC from *Rb. sphaeroides*, no changes of the spectrum of the singly-reduced Q_B could be observed (with an uncertainty of ± 5 %) in the pH-range from 4 to 8 (footnote in Graige *et al.*, 1996). One explanation for this behavior can be that the singly-reduced Q_B is protonated less than 5 % over this pH-range. According to our calculations, the singly-reduced Q_B has a protonation probability of about 30 % at pH 7.5. This result does not contradict the experimental observation, if the protonation probability of the singly-reduced Q_B remains constant at (30 ± 5) % over the pH-range from 4 to 8. This may possibly be rationalized with a special titration behavior of Q_B: Due to strong coupling of Q_B with titratable groups in the protein matrix, a nearly constant protonation probability of the singly-reduced Q_B may be maintained over a wide pH-range. It should also be kept in mind that the experiments were done with the bRC from *Rb. sphaeroides*, while we used the structure of

the bRC from *Rps. viridis* in our computation.

We found that the proton uptake by the bRC takes place before Q_B gets protonated. Due to the protonation of Q_B, the system reaches the protonation equilibrium after the first electron-transfer process. The second electron is then only transferred if Q_B is protonated. If the protonation of Q_B depends on pH, this mechanism can explain the observed pH dependence of the second electron-transfer rate. This model is similar to the one derived from kinetic studies mentioned above (Graige *et al.*, 1996).

Second Protonation of Q_B

Measurements of the energies required for the second protonation of Q_B at pH 9.0 and 9.5 gave $\geq(0\pm20)$ meV and $\geq(28\pm20)$ meV, respectively (McPherson *et al.*, 1994). Assuming a Henderson-Hasselbalch titration behavior, the protonation energy at pH 7.5 is -90 meV. This is in qualitative agreement with our calculated values of -300 meV and -410 meV (Figure 5.6). The discrepancy may be explained by the uncertainty of extrapolating the energy to lower pH-values. Furthermore, the experiments were done at the bRC from *Rb. sphaeroides*, while we considered the bRC from *Rps. viridis*. The results show that the state $Q_AQ_BH^-_{dist}$, in which Q_B is protonated at the distal quinone oxygen, is energetically more stable than the state $Q_AQ_BH^-_{prox}$. Hence, also in the doubly-reduced state of Q_B, a protonated distal oxygen is preferred to a protonated proximal oxygen.

5.3 The Electron-Transfer Reaction between Plastocyanin and Cytochrome *f*

The blue copper protein plastocyanin, designated pc, and the heme protein cytochrome *f*, designated cytf, are involved in photosynthetic electron transfer: cupriplastocyanin accepts an electron from ferrocytochrome *f*, and cuproplastocyanin donates an electron to the oxidized form of photosystem I. These proteins are well-suited to experimental and theoretical studies of protein association and electron-transfer reactions (Redinbo *et al.*, 1994; Gross, 1993; Sykes, 1991a; Sykes, 1991b; Drepper *et al.*, 1996; Haehnel *et al.*, 1994; Hervás *et al.*, 1995; Sigfridsson *et al.*, 1996). Plastocyanin contains two distinct surface patches through which it can exchange electrons with redox partners. The broad, negatively-charged acidic patch around Tyr83 is remote from the copper atom, whereas the electroneutral, hydrophobic patch around His87, a ligand to the copper atom, is proximate to this atom. Both of these important residues are somewhat exposed on the surface. Despite the different distances, these two patches are approximately equally coupled to the copper site (Kyritsis *et al.*, 1991; Sykes, 1991a; Solomon & Lowery, 1993; Ullmann & Kostić, 1995; Qin & Kostić, 1996).

The luminal part of cytochrome *f* can gently be cleaved from the short segment anchoring it as part of the cytochrome b_6f complex to the membrane. Recent crystallographic analysis of this solubilized form of cytochrome *f* revealed a remarkable two-domain structure (Martinez *et al.*, 1994). The larger domain contains a heme, with the amino group of the terminal residue Tyr1 as an axial ligand to the iron atom. The smaller domain contains a patch of positively-charged residues. Unexpectedly, the two sites are relatively far apart.

When plastocyanin and cytochrome *f* are noninvasively cross-linked in a reaction mediated by a carbodiimide (Davis & Hough, 1983), the resulting covalent complex can not detectably undergo the internal electron-transfer reaction in eq 5.2, which is fast within the electrostatic

complex (Qin & Kostić, 1992; Qin & Kostić, 1993). This unreactivity was taken as evidence that the two proteins dock and react with each other in different configurations (Qin & Kostić, 1993). The prediction and the analysis were nicely corroborated by subsequent publication of the structure of cytochrome f, which showed that the docking and the reactive configurations may not be the same. Studies of the rearrangement with complexes that plastocyanin forms with native (iron-containing) cytochrome *c* and with its zinc derivative gave evidence for configurational fluctuation, in which the docked protein molecules fluctuate around the initial docking configuration, without grossly deviating from it (Zhou & Kostić, 1992a; Zhou & Kostić, 1992c; Zhou & Kostić, 1993b; Peerey & Kostić, 1989).

Together with Ernst-Walter Knapp and Nenad M. Kostić, I investigated the association of plastocyanin and cytochrome f shown in eq 5.2 and subsequent the electron-transfer reaction shown in eq 5.3; the Roman numerals are the oxidation states of copper and iron, and the slant represents association.

$$\mathrm{pc(II)} + \mathrm{cytf(II)} \rightleftharpoons \mathrm{pc(II)/cytf(II)} \tag{5.2}$$

$$\mathrm{pc(II)/cytf(II)} \rightarrow \mathrm{pcI/cytf(III)} \tag{5.3}$$

We applied a Monte Carlo docking method combined with a molecular simulation and electrostatic calculations to this complex. This method is described in Section 2.4.

Kinetic effects of chemical modification (Anderson *et al.*, 1987; Gross & Curtiss, 1991; Christensen *et al.*, 1992) and of site-directed mutagenesis (Modi *et al.*, 1992b; Modi *et al.*, 1992a; He *et al.*, 1991) in plastocyanin indicate that this protein uses its acidic patch, and Tyr 83 in particular, for docking (eq 5.2) and the electron-transfer reaction (eq 5.3) with cytochrome f. These processes, however, are quite intricate. Replacement of Leu12 by various amino acids seems to affect the association constant, whereas neutralization of a negative charge in the mutant Asp42Asn seems not to, even though residue 12 lies in the hydrophobic patch and residue 42 lies in the acidic patch. Moreover, the mutation Phe35Tyr in the hydrophobic patch, not far from Leu12, appears not to affect the association constant (Modi *et al.*, 1992b). Mutations of residue 12 may affect the reaction indirectly, by perturbing the redox potential of the nearby copper site (Sigfridsson *et al.*, 1996). Conclusive analysis of kinetic effects of mutation requires direct observation of the intracomplex electron-transfer reaction in eq 5.3; this can be achieved at low ionic strength (Qin & Kostić, 1992; Qin & Kostić, 1993). Effects of mutation on bimolecular rate constants determined at intermediate ionic strengths can perhaps be partitioned into contributions from the two steps of the reactions described in eqs 5.2 and 5.3, but this partitioning may be uncertain. A small but intriguing dependence of the electron-transfer rate constant on ionic strength may be due to a mismatch between thermodynamic stability and redox activity of a diprotein complex formed at low ionic strength and to a rearrangement at higher ionic strength (Meyer *et al.*, 1993). Alternative explanations are conceivable. The small dependence may be due to a reaction between the diprotein complex and free plastocyanin or cytochrome f. It could perhaps be explained in terms of different contributions by the monopoles, dipoles, and higher multipoles to the electrostatic interaction energy at different ionic strengths. Such an explanation has been offered (Watkins *et al.*, 1994), and a similar one can be attempted by van Leeuwen theory (van Leeuwen, 1983). A recent study of plastocyanin mutants found that the upper cluster of anionic residues (nos. 59-61) is not involved in the electron-transfer reaction, but that the lower cluster (nos. 42-45) is (Lee *et al.*, 1995a).

The aforementioned studies show how intricate the problem of association and reaction of plastocyanin and cytochrome f is. The acidic patch in the former and the basic patch in the

latter are important for the reaction. It is not clear, however, whether the prominent residue Tyr83 is involved in the docking, in the reaction, or in both. I will discuss this question below.

5.3.1 Covalency of Copper-Ligand and Iron-Ligand Bonds

Electronic structure of the cupric site in plastocyanin is relatively well understood (Penfield *et al.*, 1981; Solomon *et al.*, 1992; Solomon & Lowery, 1993; Penfield *et al.*, 1985; Larson *et al.*, 1995). The short and highly covalent bond between the copper(II) atom and the thiolate anion of Cys84 provides strong electron coupling to Tyr83, a residue in between the two anionic clusters at the acidic patch. The ligand His87, partially exposed at the hydrophobic surface, also provides a good path for electronic tunneling to the copper (II) atom. Indeed, both surface sites are well coupled electronically with the copper atom. We will discuss later their roles in electron tunneling.

In order to get an estimate of the electronic structure of the heme center, we performed an extended Hückel calculation (Hoffmann, 1963; Zerner *et al.*, 1966). Iron-Ligand bonding in Cytochrome f coordinates of the heme were taken directly from the protein structure. All the peripheral substituents in the porphyrin were retained; the two cysteine side chains that form covalent bonds to the porphyrin were represented with methylthio groups; the imidazole group of histidine and the terminal amino group binding in the axial positions to the iron were represented with an imidazole and a methylamine, respectively; and both propionate groups were reasonably deprotonated.

Our simple calculation, by the extended Hückel method, seems to be the first quantum-chemical study of the unusual heme complex found in cytochrome f. The several highest filled molecular orbitals have similar energies. The HOMO is delocalized over the porphyrin ring; the three molecular orbitals just below it are mostly composed of the iron 3d orbitals. These high-lying molecular orbitals have very small contributions from the two axial ligands. Our finding that electron transfer in cytochrome f involves mainly the π electron system agrees with similar findings by others concerning other cytochromes (Nakagawa *et al.*, 1994; Stuchebrukhov & Marcus, 1995). Indeed, a porphyrin-to-iron charge-transfer transition is observed spectroscopically (Gadsby & Thomson, 1990).

5.3.2 Diprotein Complex Configuration for Each of the Six Families

The series of calculations culminating in Table 5.2 began with 32,000 Monte Carlo trajectories obtained with rigid proteins. Approximately 5,000 of them ended at local minima of energy. Of these, 140 configurations were further considered and clustered into six families on the basis of structural similarity. The most stable member of each family was used as starting point of a molecular dynamics simulation, in which the protein molecules were hydrated and given conformational flexibility. Finally, the energy of each configuration was energy minimized. They are designated A through F. The details of the procedure are described in Section 2.4.

The criterion for a salt bridge between a carboxylate anion in plastocyanin and an ammonium cation in cytochrome f was the O$\cdots$N distance of 3.2$\cdots$3.6 Å. Such interactions are found only in configuration F, between Asp42 and Lys65 and between Asp44 and Lys65. This scarcity of salt bridges is understandable because they are energetically less favorable than hydration of both ions (Hendsch & Tidor, 1994; Dougherty, 1996; Waldburger *et al.*, 1995). In simulations in which the solvent water is not considered, salt bridges are commonly found, and their contribution to the stability of the complex is usually overestimated. In our simulation, in which

configuration	Cu-Fe distance (Å)	interacting side chains	
		anions in pc	cations in cytf
A	34	Glu59, Glu60, Glu61	Lys187, Lys185
		Asp44, Glu43, Glu45	Lys65, Lys66
B	31	Glu59, Glu60	Lys185, Lys187
		Glu43	Arg209, Lys45
C	37	Glu59	Lys187
		Asp45, Glu43	Lys65, Lys66, Lys58
D	14	Glu43, Asp42, Asp44, Glu45	Lys187, Arg209
		Glu59, Glu60	Lys65, Lys58
E	20	Asp44, Glu45, Asp42, Glu43	Lys187, Arg209
		Glu59, Glu60, Glu61	Lys58, Lys65, Lys66
F	35	Asp42, Asp44, Glu43	Lys58, Lys65
		Glu59, Glu60, Glu61	Arg209, Lys187

Table 5.2: Six configurations of the diprotein complex that emerged from Monte Carlo calculations, molecular dynamics simulations with allowance for flexibility and with inclusion of water, and energy minimization.

water is explicitly treated, salt bridges occur only in buried regions of the protein interface. The ionic side chains located in the exposed regions prefer to be hydrated, if they are allowed to.

Despite the scarcity of salt bridges, there are numerous electrostatic attractions, listed in Table 5.2. Two oppositely charged ions were considered interacting if the carbon atom of the carboxylate ion approached the nitrogen atom of the ammonium or guanidinium cation at less than 8.0 Å. This distance is included by the radii of the ions and the thickness of the water layer.

Only in the configurations D and E is the copper-iron distance shorter than 30 Å. As Figure 5.7 shows, in the other four configurations the copper atom points away from the heme.

The prominent residue Tyr83 lies outside of the protein interface and is not involved in docking in the configuration B. This residue lies at the edge of the interface in the configuration A and is buried in the interface in the remaining four configurations, C through F. In three of them Tyr83 appears to form a hydrogen bond with the following residues of cytochrome f: Arg209 in the configurations D and F, and Lys65 in the configuration E. This last interaction will be discussed in some detail below.

Cytochrome f contains three loops at the surface region through which it binds to plastocyanin: Lys185-Gly189, Pro208-Glu212, and Leu61-Lys65. These sections of the protein chain show large temperature factors in the crystal structure, an indication that they are mobile. Molecular dynamics simulations revealed that association with plastocyanin causes slight reorientation of these loops in nearly all of the six configurations. The antiparallel β-sheet Gly157-Asn167 in the configuration D swings by as much as 8 Å. Molecular dynamics simulations showed no large structural changes in plastocyanin in any of the six configurations.

5.3.3 Energetics of the Docking and Analysis of the Stability of the Six Configurations

Different contributions to the energy of the diprotein complex are defined in eqs 2.38, 2.40, 2.41, 2.42, and 2.43 and shown in Table 5.3. No single component of the docking interaction

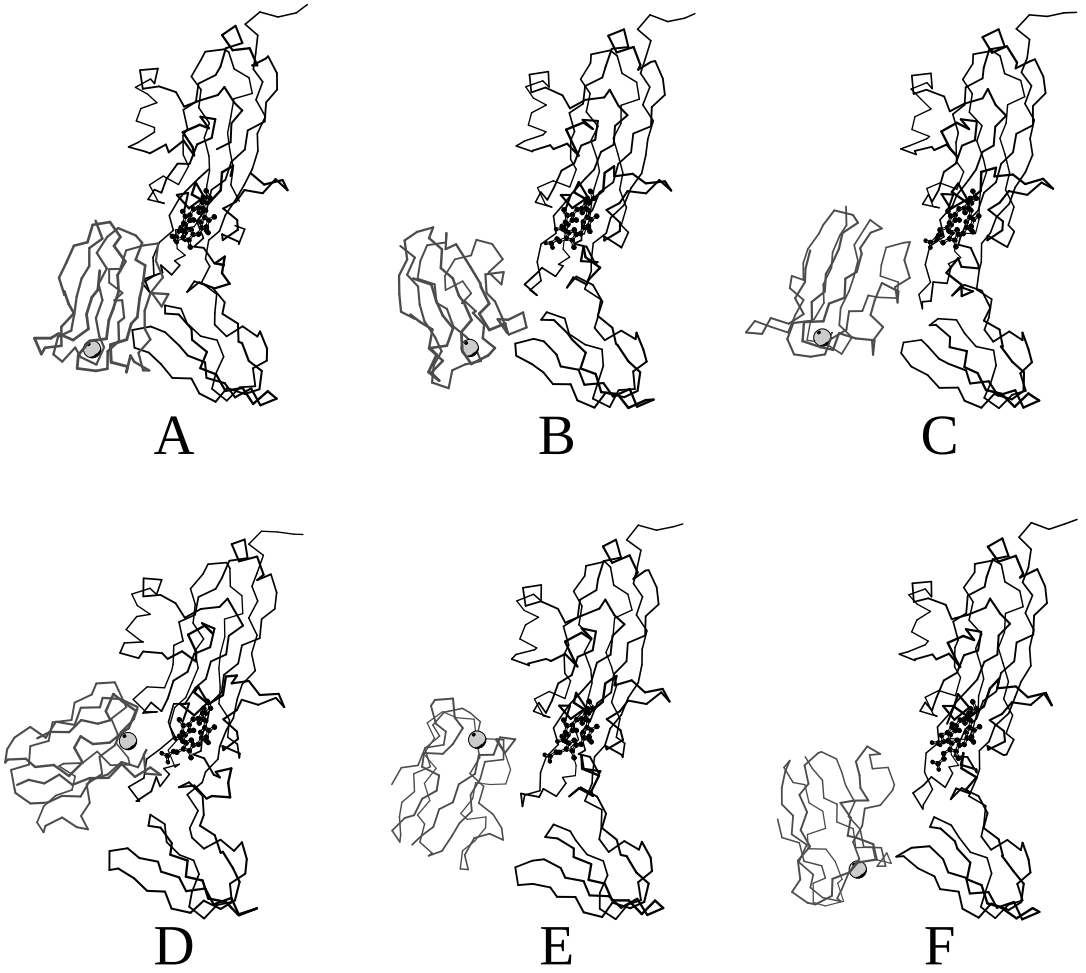

Figure 5.7: The optimized six configurations of the diprotein complex between plastocyanin and cytochrome f that emerged from molecular dynamics simulations for 260 ps and energy minimization. In the simulations hydration was treated explicitly, and conformational flexibility was allowed. The copper atom and the heme are highlighted.

configuration	$\Delta\Delta G_R$ reaction field	ΔG_c coulombic	ΔG_{NE} nonelectrostatic	ΔG_E [a] electrostatic	ΔG_T [b] total
A	1483	-2851	-120	-1368	-1488
B	2112	-3975	-94	-1863	-1957
C	2572	-4289	-116	-1717	-1833
D	2676	-4394	-157	-1718	-1875
E	2713	-4585	-107	-1872	-1979
F	3139	-4752	-99	-1613	-1712

$a - \Delta G_E = \Delta\Delta G_R + \Delta G_C$

$b - \Delta G_T = \Delta\Delta G_R + \Delta G_C + \Delta G_{NE} = \Delta G_E + \Delta G_{NE}$

Table 5.3: Energies (in kJ/mol) of the complex between plastocyanin and cytochrome f calculated with ε_s=2.0 and b=20.0 cal/Å^2.

correlates with the calculated total energies, ΔG_T. Stabilities of different configurations can be properly analyzed only by recognizing the interplay of the different energy contributions.

If only Coulomb energies was considered, configuration F would be the most stable one. When, however, the change in the reaction field is taken into account, this configuration becomes distinctly unfavorable. This destabilizing contribution of the reaction field may be due to the presence of two salt bridges, discussed above. This example clearly shows the peril of analyzing protein complexes solely, or mostly, in terms of Coulomb interactions even when the proteins are highly charged. Although this approach to molecular modeling remains popular (Roberts *et al.*, 1991; Adir *et al.*, 1996), non-Coulomb contributions to electrostatic energy should be considered as well.

As Table 5.3 shows, the non-electrostatic term is less than 10 % of the electrostatic term, but it should be taken into account too. It makes a significant contribution to the total energy of the configuration D.

The configuration B has a relatively small interface, a sign for loose packing of the two proteins. Consequently, its non-electrostatic term is the smallest of all in Table 5.3. Since Tyr83 is not involved in docking and since the metal atoms are far apart, this configuration probably is unimportant in the electron-transfer reaction. Configurations A and C, which have the longest copper-iron distances, are likewise of less interest.

The most stable configuration, E, owes its stability largely to the very favorable electrostatic energy. This finding is consistent with kinetic experiments, which showed a marked dependence of the rate constants for the reaction in eqs 5.3 on ionic strength (Qin & Kostić, 1992; Meyer *et al.*, 1993)

5.3.4 Interactions of Tyr83 with Cytochrome f Residues

The hydroxyl group of Tyr83 in plastocyanin emerges from several simulations as acceptor in hydrogen bonds. The donors in these hydrogen bonds, from cytochrome f, are Lys65 in the most stable configuration, designated E, and Arg209 in the configurations D and F. Because these donors are cations, we were intrigued by the possibility that the putative hydrogen bonds are in fact interactions between cation and the aromatic ring, so-called cation-π interaction (Kumpf & Dougherty, 1993; Dougherty, 1996).

Pyramidal complexes between aromatic molecules and cations such as Ag^+ have long been known. These surprisingly strong, noncovalent interactions are being increasingly emphasized in studies of enzyme-substrate interactions and of molecular recognition in synthetic host-guest systems (Dougherty, 1996; Sussman & Silman, 1992). A pair of hydrated ions is more stable than a salt bridge between them, but a single cation is more stable in a complex with an aromatic molecule than when it is hydrated (Kumpf & Dougherty, 1993; Waldburger *et al.*, 1995; Dougherty, 1996). Unfortunately, state of the art in molecular mechanics calculation is inadequate for a correct description of cation-π interactions; their energies are greatly underestimated (Dougherty, 1996; Caldwell & Kollman, 1995; Kumpf & Dougherty, 1993). Satisfactory force fields must include contributions from polarization, induced dipoles, dispersion forces, charge transfer, and possibly other interactions and processes (Kim *et al.*, 1994; Lee *et al.*, 1995b). Such calculations are still in its infancy and are applied so far to small molecules only (Caldwell & Kollman, 1995). Applications to proteins, let alone structural optimization of protein complexes, are challenges for the future.

The probability of this strong interaction between plastocyanin and cytochrome f impelled us to a broader analysis of our findings about of docking (here) and about electron transfer

pc/cytf	10^{-20} (relative coupling)^2 for the best path					
config-	no H_2O, isotropic		H_2O, isotropic		H_2O, anisotropic	
uration	ε=0.6	ε=1.0	ε=0.6	ε=1.0	ε=0.6	ε=1.0
A	310	3.9×10^{3}	310	3.9×10^{3}	65	825
B	3.6×10^{-3}	0.078	8.1	62	1.2×10^{-3}	8.9×10^{-3}
C	7.6	79	7.6	79	0.2	2.2
D	1.8×10^{11}	1.4×10^{12}	2.4×10^{12}	2.4×10^{12}	2.2×10^{9}	1.7×10^{10}
E	7.7×10^{6}	5.9×10^{7}	2.8×10^{7}	1.5×10^{8}	4.4×10^{5}	3.4×10^{6}
F	44	950	44	950	1.2	26.5

Table 5.4: Best electron-tunneling paths from Fe(II) to Cu(II) in six configurations, shown in Figure 5.7, of the plastocyanin/cytochrome *f* complex calculated for two levels of hydration with two parametrizations of the coupling within the aromatic rings (ε Values) and considering of the metal-ligand covalency as isotropic or anisotropic

(below). The observed 40-fold decrease of the bimolecular rate constant upon the mutation Tyr83Leu (Modi *et al.*, 1992b) is consistent with a decrease in the binding affinity. Attribution of this decrease, wholly or in part, to a changed electron-transfer ability is a matter of kinetic analysis, which is further complicated by the possibility of the rearrangement of the protein complex.

5.3.5 Electron-tunneling Paths

The method *Pathways* (Onuchic *et al.*, 1992) is applicable to electron-transfer systems in which the main consideration is the nature of the matter between the donor and the acceptor, not solvation and other effects. We applied it to the complex between plastocyanin and cytochrome *c*, in which both redox sites are enclosed in the protein matter (Ullmann & Kostić, 1995). As in this previous study, trends, not absolute values, in the quantities t_{DA}^2 for various paths were considered.

Table 5.4 shows that the configuration D, which has the shortest copper- iron distance, also has by far the strongest electronic coupling between the two metal sites, i. e., it possesses the most efficient path. Next comes the configuration E, with a longer distance and a less strong coupling. The other four configurations seem to be unfavorable for electron transfer. Inclusion of water slightly enhances the coupling in three of these four configurations and greatly enhances it in the configuration B. The small interface in configuration B (see above) benefits from hydration; the best, but still inefficient, path includes three water molecules. Generally speaking, paths via multiple water molecules are unlikely because positions of these molecules must be simultaneously favorable for electron transfer to occur.

Because of the approximations in the *Pathways* method, even the relative magnitudes of the couplings in Table 5.4 must be taken skeptically. More efficient paths may be discovered by more rigorous calculations. We sought additional paths by widening the search to include relative couplings lower than those in the best path for each of the configurations D and E. The results are given in Table 5.5. The best of all paths, which occurs in the configuration D, is shown in Figure 5.8. Between a propionate group of the heme and Pro86 in plastocyanin there is a van der Waals contact. Depending on the treatment of copper(II)-ligand bonding, this path can take somewhat different direction to the copper(II) atom, but always within the short

Configuration	Acceptor	blocked	(relative coupling)^2	($\gamma_{AL}^2 \times$ relative coupling)^2	path
D	Cu	none	2.4×10^{-8}	4.5×10^{-13}	Fe-Tyr1-H_2O-His87-Cu
		Tyr1	1.4×10^{-8}	2.0×10^{-12}	Fe-Heme-Pro86-His87-Cu
		Sol	1.4×10^{-8}	2.0×10^{-12}	Fe-Heme-Pro86-His87-Cu
		Sol/Pro86	8.0×10^{-10}	1.7×10^{-10}	Fe-Heme-Ser85-Cys84-Cu
E	Cu	none	1.5×10^{-12}	2.2×10^{-16}	Fe-Heme-H_2O-H_2O-Gln88-His87-Cu
		His87	1.6×10^{-13}	3.4×10^{-14}	Fe-Heme-H_2O-H_2O-H_2O-Ser85-Cys84-Cu
		Gln88	2.2×10^{-12}	3.2×10^{-16}	Fe-Heme-H_2O-H_2O-H_2O-Gln88-His87
		Heme	1.3×10^{-12}	2.4×10^{-17}	Fe-Tyr1-H_2O-Gly89-Gln88-His87-Cu
		H_2O	6.0×10^{-13}	1.1×10^{-17}	Fe-Tyr1-Gly89-Gln88-His87-Cu
		H_2O, Gln88	4.4×10^{-14}	8.2×10^{-19}	Fe-Tyr1-Gly89-His87-Cu
	Lys65-Tyr83	unblocked	1.8×10^{-13}	–	Fe-Heme-Asn70-Leu69-Ala68-Gly67-Lys66-Lys65-Tyr83
		Asn70	7.6×10^{-14}	–	Fe-Heme-H_2O-Ala68-Gly67-Lys66-Lys65-Tyr83
		Heme	2.2×10^{-14}	–	Fe-Tyr1-H_2O-H_2O-H_2O-H_2O-H_2O-Lys65-Tyr83
E'[a]	Cu	none	1.1×10^{-13}	2.0×10^{-18}	Fe-Tyr1-H_2O-H_2O-Gly89-Gln88-His87-Cu
		H_2O	3.6×10^{-17}	5.2×10^{-21}	Fe-Heme-Arg156-Leu61-Gln88-His87-Cu
		His87	1.4×10^{-14}	3.0×10^{-15}	Fe-Heme-H_2O-H_2O-H_2O-Ser85-Cys84-Cu
		His87, H_2O	9.6×10^{-18}	2.0×10^{-18}	Fe-Heme-Arg156-Leu61-Gln88-Cys84-Cu
	Lys65-Tyr83	none	1.6×10^{-12}	–	Fe-Heme-Arg156-Val60-Leu61-Lys65
		Arg156	1.7×10^{-13}	–	Fe-Heme-Asn70-Leu69-Ala68-Gly67-Lys66-Lys65-Tyr83

a – Partial optimization. Coordinates taken from the MD trajectory of configuration E after 70 ps.

Table 5.5: Extended search for electron transfer paths less efficient than those included in Table 5.4 takes a long time and requires much memory. To make it more efficient, we systematically "removed" from the best paths certain amino-acid residues or just their side chains by neglecting the coupling interactions involved. The results are given in this table.

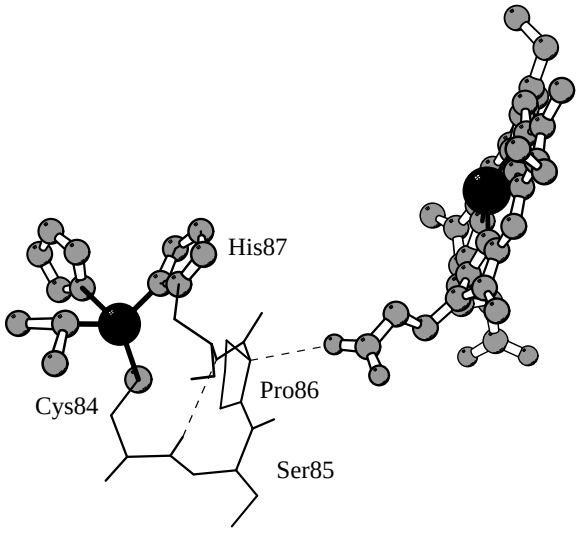

Figure 5.8: The most efficient electron-tunneling path in the complex between the cupric site in plastocyanin (left) and the ferroporphyrin group in cytochrome f (right) calculated by the *Pathways* method. This path was found in the configuration D of the diprotein complex.

protein dielectric constant, ε_s	b in eq 2.40	$\Delta\Delta G_E$	$\Delta\Delta G_{NE}$	$\Delta\Delta G_T$
1.0	5	323	-12	311
	6.8	323	-17	306
	20	323	-50	273
2.0	5	154	-12	142
	6.8	154	-17	137
	20	154	-50	104
4.0	5	72	-12	60
	6.8	72	-17	55
	20	72	-50	22

Table 5.6: Differences in electrostatic, nonelectrostatic, and total energies (in kJ/mol) between the configuration D, having the best heme-copper coupling, and the configuration E, Having the lowest total energy.

segment 84-87. If the anisotropy of the copper bonding is ignored, the path goes via covalent bonds, through His87. If the strong coupling of Cys84 to copper(II) is recognized, the path goes via Ser85 and Cys84. This example shows the intricacies of analyzing electron-tunneling paths at their beginnings and ends, near the donor and acceptor sites.

5.3.6 Comparison of the Configurations D and E

The configuration E emerged as the most stable one (Table 5.3), whereas the configuration D turned out to be the most reactive one with respect to inter molecular electron transfer (Table 5.4). Because of the importance of this difference for the analysis of the reaction in eq 5.3, we checked whether the relative stabilities change when different parameters are used in the energy calculations.

Dielectric properties of proteins depend on reorientation of permanent and induced dipoles. Much has been written about the value dielectric constant in proteins (Harvey, 1989; Warshel & Russel, 1984; Warshel & Åqvist, 1991). The value 4.0 is appropriate for proteins if ionic residues are treated as point charges; this value is used most often (Harvey, 1989; Gilson, 1995; Honig & Nicholls, 1995). Atomic charges in the CHARMM program are adjusted for a dielectric constant of 1.0 can be used in molecular dynamics simulations. If the protein environment is rigid, as for instance for the special pair in the photosynthetic reaction center, the value ε_S=1.0 was most suitable to reproduce certain experimental results (Muegge *et al.*, 1996). Therefore, we used also this value. With the aforementioned parameterization of charges, CHARMM implicitly recognizes reorganization of induced, but not of permanent, dipoles. Since both of these effects contribute nearly equally to the value of the dielectric constant, the value ε_S=2.0 seemed to be the most realistic. The results in Table 5.3 were obtained with this value. Three different values of the parameter b in eq 2.40 were tested.

Results of these exploratory calculations are shown in Table 5.6. The variation of the parameters ε and b did not change the main finding – the configuration having the best electronic coupling between the copper and heme sites (D) is different from the configuration with the greatest affinity for protein association (E).

5.3.7 Possible Involvement of Tyrosine 83 and Cationic Side Chains in Electron Transfer

It is important to keep in mind the approximations embodied in the *Pathways* method. In this and in other methods for estimating electronic coupling an effective two-state Hamiltonian based on a pertubation approach is used to describe the interactions between the donor and the acceptor. This description becomes invalid if the electronic states of the "bridging" groups (those interposed between the donor and the acceptor) strongly interact with the donor state or the acceptor state. If the electron-transfer reaction involves a third intermediate, the description in terms of the superexchange mechanism fails also (Marcus & Sutin, 1985; Larson, 1981; Larson, 1983; Skourtis & Mukamel, 1995).

If, as discussed above, a cationic side chain in cytochrome f and the aromatic ring of Tyr83 in plastocyanin form a special bond, then the LUMO of this so-called charge-π complex may act as an electron acceptor, so that a radical intermediate is formed in the course of electron transfer from the ferroheme to the cupric site. Indeed, recent quantum-chemical calculations showed that interaction of a σ^* orbital of ammonium cation and a π orbital of benzene plays an important role in stabilizing this pair (Lee *et al.*, 1995b; Kim *et al.*, 1994). The LUMO is delocalized over the whole complex and is well suited to accept the electron in the hypothetical intermediate.

To our knowledge, a radical of unmodified Tyr83 has not been detected in studies of electron-transfer reactions. Most of these studies, however, were done with reducing agents that are not expected to form the special interaction to the aromatic ring of Tyr83. We postulate it for the reaction with the physiological partner, cytochrome f. In the few studies of this reaction, radical intermediates were not considered. A short-lived intermediate may be possible, and this question is worthy of an experimental study.

If a radical intermediate is involved in the electron transfer, then the analysis by the *Pathways* method must be done in two parts – from ferroheme to Tyr83 and from Tyr83 to the cupric site. Because state of the art in molecular mechanics is inadequate for a description of interactions between cations and aromatic rings (see above), we did not restrict our analysis to optimized configurations. We considered also the structures of the diprotein complex at the earlier stages of simulation and the actual structures of plastocyanin and cytochrome f. The main result of this analysis is the interesting pattern shown in Figure 5.9 and in Table 5.5.

A tunneling path starts at the iron atom and goes through the porphyrin ring, via a salt bridge involving the propionate group in the pyrrole ring D and the guanidinium group of Arg156, via another hydrogen bond to the oxygen atom in Val60, via the peptide bond to Leu61, then to the oxygen atom in Lys65, and then to the ammonium cation in the side chain that presumably interacts with the aromatic ring in Tyr83. This pattern is present in the early stages of simulation of the configuration E, but disappears after approximately 80 ps. Since, however, the aforementioned hydrogen bonds are evident in the crystal structure of cytochrome f (Martinez *et al.*, 1994) we believe that their disappearance is caused by the inability of the force field to recognize the special interaction of Lys65 and Tyr83. Instead of simulating this interaction, the force field simulates others that are more tractable, such as the attraction of Lys65 to the acidic patch in plastocyanin; see Table 5.2. From this point of view "diversion" of Lys65 creates some stress on it and on residues bound to it; consequently the aforementioned hydrogen bonds and the path requiring them are disrupted. Then a path along the backbone of cytochrome f, from Asn70 to Lys65, becomes relatively favorable, with a coupling of approximately 10 % of the previous one, see Figure 5.9.

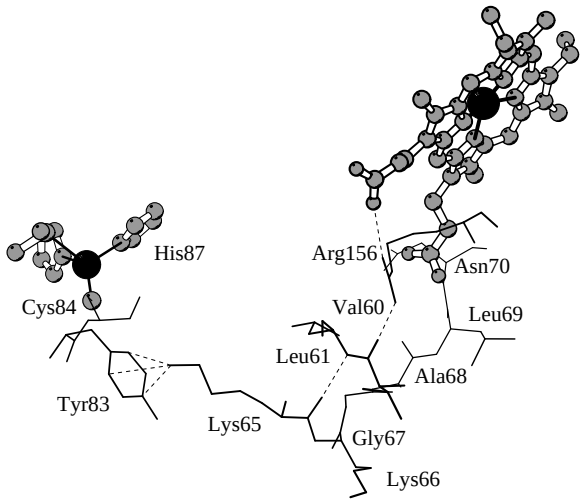

Figure 5.9: Two special electron-tunneling paths between the cupric site in plastocyanin (left) and the ferroporphyrin group in cytochrome *f* (right) found in the configuration E of the diprotein complex. The ammonium cation of Lys65 is shown above the aromatic ring of Tyr83, in a so-called cation-π interaction. One path (through the residues 156, 60, 61, and 65) involves the hydrogen bonds (dashed lines), whereas the other path leads through the protein backbone (residues 70 to 65). Tyr83, Cys84, and His87 belong to plastocyanin, the rest to cytochrome *f*

This diprotein system, and likely others in which interactions between cationic and aromatic side chains may occur, should be thoroughly investigated in the future. Quantum-mechanical calculations should be combined with classical mechanical simulations based on improved force fields to analyse these newly-recognized interactions.

5.3.8 Electron-Transfer Inactivity of the Covalent Diprotein Complex

In the presence of carbodiimides, direct amide bonds form between lysine side chains in cytochrome *f* and carboxylate groups in glutamate or aspartate side chains in plastocyanin (Davis & Hough, 1983). Structures and redox properties of the active sites of these proteins are not significantly perturbed (Morand *et al.*, 1989), but the intracomplex electron-transfer reaction (eq 5.3), which is fast in the noncovalent complex, is undetectably slow in the covalent complex (Qin & Kostić, 1993). This finding lead to the suggestion, that a rearrangement of the initially formed, electrostatic complex is necessary for the electron transfer and that cross-links prevent this rearrangement (Qin & Kostić, 1993). Indeed, rearrangement processes are important in electron-transfer reactions of various protein complexes (Zhou & Kostić, 1993b-Ivković-Jensen & Kostić, 1997). In a recent theoretical study (Ullmann *et al.*, 1997b), we proposed a structural model of the rearrangement in the plastocyanin-cytochrome *f* complex. The direct cross-links (without any tethers) make the covalent complex rigid and preclude the rearrangement, shown in Figure 5.10, from the most stable configuration (E) into the most reactive one (D). This rearrangement is possible in the case of the noncovalent complex, which is flexible. Beside this possible explanation, we gave also an alternative interpretation of the redox-inactivity of the cross-linked complex (Ullmann *et al.*, 1997b). We proposed a cation-π interaction between the side chains of Lys65 in cytochrome *f* and Tyr83 in plastocyanin. Such

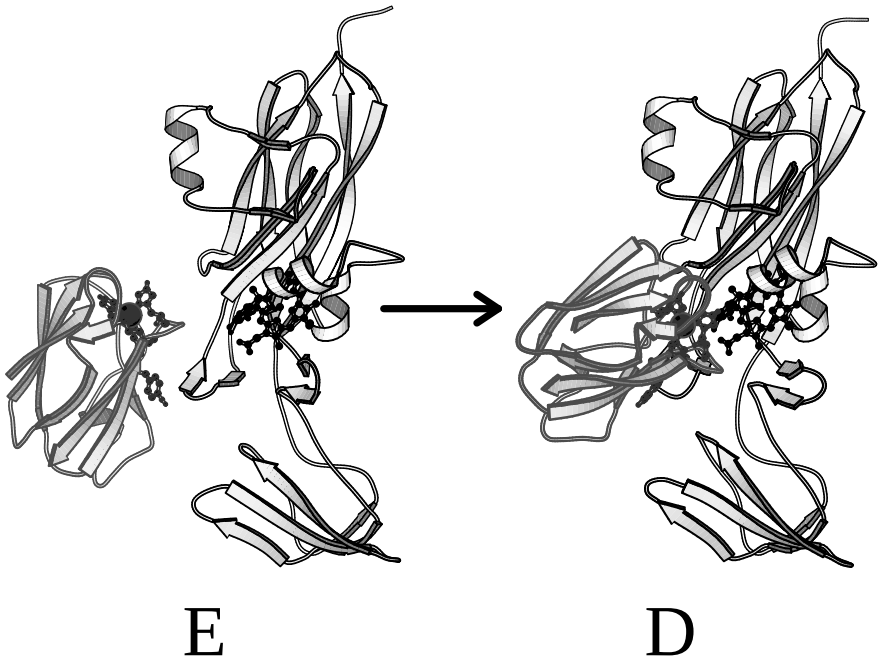

Figure 5.10: Rearrangement of the diprotein complex between cupriplastocyanin and ferrocytochrome *f* that may be involved in the intracomplex electron-transfer reaction. The configuration E has the lowest binding affinity, whereas the configuration D provides the best electronic coupling between the redox sites, which are highlighted.

interactions have recently been documented in synthetic host-guest adducts and biochemical complexes (Dougherty, 1996, Ma & Dougherty, 1997), but we are not aware of any investigations of the electrochemical properties of such complexes. However, the system composed of the cation over the aromatic ring may serve as an intermediate electron acceptor in the protein complex, since the cation can stabilize an anionic radical at the aromatic ring. If so, the electron-transfer reaction could occur in two steps. An electron is first transferred from the ferroheme in cytochrome *f* to the aromatic ring of the cation-π system at the protein-protein interface, and then from the transient anion-radical to the copper site in cupriplastocyanin. The two-step reaction can be faster than the corresponding one-step reaction, if each step is considerably faster than the assumed one-step reaction. The electronic coupling between the heme and the copper site in the plastocyanin-cytochrome *f* complex may be too weak to allow the fast reaction that is observed experimentally.

The redox-inactivity of the cross-linked complex can be explained in terms of the two-step mechanism. Cross-linking of Lys65 to an acidic residue disrupts the cation-π interaction between Lys65 and Tyr83. Indeed, the residues Glu59 and Glu60 of plastocyanin, which have been implicated in covalent cross-linking between the two proteins (Morand *et al.*, 1989), lie near Lys65 in the calculated configuration of the plastocyanin-cytochrome *f* complex (Ullmann *et al.*, 1997b). Under this hypothesis, the diversion of Lys65 away from Tyr83 would disturb the electron-transfer path and neutralize the cation required for the stabilization of the anion radical of Tyr83.

The hypothesis of a cation-π interaction and of its special role in the electron-transfer mechanism can be tested by analyzing its consistency with the available amino acid sequences. The

residue Tyr83 is conserved in nearly all plastocyanins; it is only replaced by a phenylalanine in two algal plastocyanins. But Lys65 is missing in all cyanobacterial cytochrome *f* sequences and in two eukaryotic algal cytochromes *f*. These two eukaryotic algae belong to the taxonomic groups *Rhodophyta* (red algae) and *Glaucophyta*, which have rather primitive chloroplasts with many similarities to cyanobacteria (Köhler *et al.*, 1997). The lack of Lys65 does not necessarily invalidate the proposal, that a cation-π system serves as a "half-way" electron acceptor in the interprotein reaction. The role of Lys65 may be fulfilled by Lys66, which is conserved in all known cytochrome *f* sequences.

Lysine side chains are not the only cations potentially capable of interacting with the aromatic π-systems of Tyr83 in plastocyanin. Alternatively, both the cation and the aromatic residue may belong to the same protein. The residue at position 88, which is located above the aromatic ring in plastocyanin, is an arginine in all known cyanobacterial plastocyanins. Their interaction could conceivably form a cation-π system within plastocyanin. This hypothesis is supported by a recent NMR spectroscopic model of a cyanobacterial plastocyanin (Badsberg *et al.*, 1996). When Lys65 is present in cytochrome *f*, it may interact with Tyr83 in plastocyanin, and a cation-π system exists at the protein-protein interface. When Lys65 is laking in cytochrome *f*, Arg88 and Tyr83 in plastocyanin may form a cation-π system within this protein. In either case the interprotein electron-transfer reaction can occur in two steps, because Tyr83 is always involved in a cation-π system. The electron transfer in the cyanobacterial plastocyanin-cytochrome *f* complex may go via the serine or the glutamine, which replaces Lys65 in cyanobacterial cytochrome *f*. This serine or glutamine residue is a capable hydrogen-bond partner of Arg88 in cyanobacterial plastocyanin. We have found no amino-acid sequence that disagrees with this expanded version of the hypothesis.

A cyanobacterial cytochrome *f* seems to react differently with plastocyanins from the same cyanobacterium and from spinach, a higher plant. A recent kinetic study (Wagner *et al.*, 1996) showed, that the former reaction is fast while the latter is very slow at medium ionic strength. Moreover, the former reaction becomes slower and the latter faster as ionic strength is raised. These observations were qualitatively interpreted in terms of electrostatic screening, since plastocyanin from spinach and from this cyanobacterium bear a different total charge (Wagner *et al.*, 1996).

These findings, however, may be also consistent with the assumption discussed above, that a two-step mechanism for the electron transfer involving a cation-π system is more favorable than a one-step mechanism. The cation-π complex is present within cyanobacterial plastocyanin, as discussed above. In this case, the electron-transfer reaction may be relatively fast because of it. A cation-π interaction is unlikely within spinach plastocyanin, because this protein lacks a cationic side chain in the correct position with respect to Tyr83 and also unlikely between this plastocyanin and cyanobacterial cytochrome *f*, because the latter lacks Lys65. Thus, the electron-transfer reaction in this protein complex may be relatively slow, because it can not use the cation-π system as an intermediate state.

5.4 Comparison of the Isofunctional Electron-Carrier Proteins Plastocyanin and Cytochrome c_6

In cyanobacteria and some eukaryotic algae, the heme protein cytochrome c_6 can replace plastocyanin under conditions of copper deficiency (Redinbo *et al.*, 1994). While the electron-transfer reactions of plastocyanin with various partners have been studied extensively in recent years (for

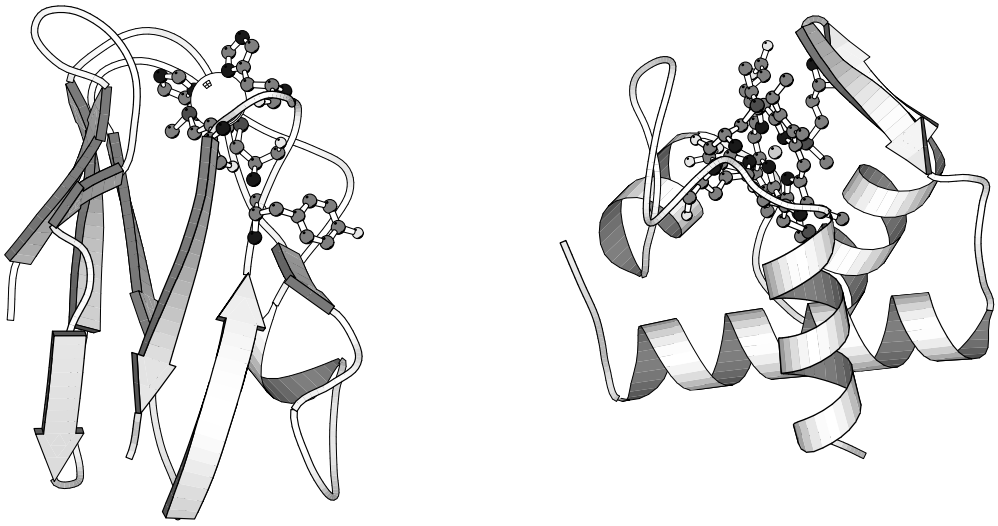

Figure 5.11: Structures of plastocyanin and cytochrome c_6. Although the structure of both proteins is completely different, both have the same function in the photosynthetic electron-transfer chain.

review see Redinbo *et al.*, 1994; Sykes, 1991a; Sykes, 1991b), only a few studies examined the electron-transfer reactions of cytochrome c_6 (Hervás *et al.*, 1995; Hervás *et al.*, 1996; Navarro *et al.*, 1997 and references cited therein).

The structure of plastocyanins from various species has been analyzed by X-ray crystallography and NMR spectroscopy (see Redinbo *et al.*, 1994 for review). Recently, the structure of cytochrome c_6 from three species has been determined (Frazão *et al.*, 1995; Kerfeld *et al.*, 1995; Banci *et al.*, 1996; Beissinger *et al.*, 1998). In the case of *Chlamydomonas reinhardtii*, the structure of plastocyanin (Redinbo *et al.*, 1993) and of cytochrome c_6 (Kerfeld *et al.*, 1995) are known. The two proteins show completely different secondary and tertiary structures. Plastocyanin has a beta-barrel fold, while cytochrome c_6 has a mainly α-helical fold (Figure 5.11). Since, however, cytochrome c_6 can replace plastocyanin in the cell, the two proteins should have similar surface patterns for the recognition of cytochrome *f* and photosystem I. Indeed, both proteins have a hydrophobic and an acidic patch on their surface (Frazão *et al.*, 1995; Kerfeld *et al.*, 1995). The acidic patch in plastocyanin consists of two distinct clusters formed by residues 42-44 and residues 59-61 respectively. In some plastocyanins, including that from *Chlamydomonas reinhardtii*, two additional acidic residues (residue 53 and 85) are located within the acidic patch (Redinbo *et al.*, 1994). In the case of plastocyanin, the hydrophobic and the acidic patch are involved in physiological reactions (Redinbo *et al.*, 1994; Sykes, 1991a; Sykes, 1991b). An electron is transferred from the copper site of plastocyanin to $P700^+$ of photosystem I via the hydrophobic patch (Haehnel *et al.*, 1994). The electron-transfer path from the heme site of cytochrome *f* to the copper site of plastocyanin seems to involve the highly-conserved residue Tyr83 (He *et al.*, 1991; Modi *et al.*, 1992b), which is located in the acidic patch of plastocyanin. Although, Tyr83 and His87 have different distances to the copper atom, their electronic couplings to the copper site are approximately equal (Lowery *et al.*, 1993; Kyritsis *et al.*, 1991; Ullmann & Kostić, 1995; Qin & Kostić, 1996). Alternatively, the acidic patch of plastocyanin may only be involved in the docking to the basic patch of cytochrome *f*, and the electron trans-

fer could conceivably occur in a rearranged configuration via the hydrophobic patch (Frazão *et al.*, 1995; Qin & Kostić, 1993; Pearson *et al.*, 1996; Ullmann *et al.*, 1997b). We suggested recently that Tyr83 interacts with a cationic sidechain in cytochrome *f* in a special way to form a cation-π system, which might be involved in the electron-transfer reaction (Ullmann *et al.*, 1997b). In the case of cytochrome c_6, only the hydrophobic patch was suggested to be involved in electron-transfer reactions (Frazão *et al.*, 1995; Kerfeld *et al.*, 1995). A second patch on the surface of cytochrome c_6, through which cytochrome c_6 can exchange electrons, has not been identified so far.

5.4.1 Superposition of Centers of Mass, Dipole Vectors and the Hydrophobic Patches of Plastocyanin and Cytochrome c_6 from *Chlamydomonas reinhardtii*

If electrostatic interactions dominate the docking of two proteins, their association depends on ionic strength. The resulting dependence of bimolecular protein-protein reactions on ionic strength can be well described by the van Leeuwen theory (Qin & Kostić, 1996; van Leeuwen, 1983; Zhou & Kostić, 1992b; Zhou & Kostić, 1993a), in which the electrostatic potential of the proteins is approximated by its monopole and dipole. We used the same approximation for the electrostatic potentials of the two proteins to superimpose plastocyanin and cytochrome c_6. Additionally, we brought the hydrophobic patches of plastocyanin and cytochrome c_6 in proximity to each other by rotating one of them around their aligned dipole axes. A similar approach was applied by Frazão *et al.*, 1995. The total charge of cupriplastocyanin and ferricytochrome c_6 from *Chlamydomonas reinhardtii* at pH 7 is -6; their dipole moments have a magnitude of 340 D and 175 D, respectively. The Hodgkin index of this alignment is also listed in Table 2.1, for comparison.

The dipole vector of each protein was calculated with respect to its center of mass (Koppenol & Margoliash, 1982). All atomic partial charges of the proteins were considered. The origin of the coordinate system was placed on the centers of mass for both proteins, and the dipoles were aligned by rotating one molecule around the normal to the plane defined by the two dipole vectors. Next, one molecule was rotated around the aligned dipole axis to bring the hydrophobic patches of both molecules close to each other. Keeping the dipole vectors aligned, I minimized the distance between the $N_{\varepsilon 1}$ atom of His87 in plastocyanin and the inner carbon atom of the vinyl group at the heme ring C (atom CAC in the PDB convention) of cytochrome c_6. These atoms lie at the center of the respective hydrophobic patches.

Besides the total charge and the magnitude of the dipole vector, the angle between the dipole vector and the vector from the center of mass of the protein to the reaction site on the protein surface is an important parameter in the van Leeuwen theory (van Leeuwen, 1983). The angle between the dipole moment and the vector from the center of mass to the C_γ atom of Tyr83 in plastocyanin is small, in *Chlamydomonas reinhardtii* it is 19^o. Therefore we searched for an aromatic residue in cytochrome c_6 lying at a small angle with respect to the dipole moment. We found Tyr51, which lies at an angle of 23^o with respect to the dipole moment.

As Figure 5.12 shows, both Tyr51 in cytochrome c_6 and Tyr83 in plastocyanin are surrounded by negatively charged residues. The residues in these two proteins which may have a similar function in the recognition of the reaction partners are listed in Table 5.4.1. Two residues are considered to be isofunctional, if the distance of their acidic groups in the superposition is less than 6.5 Å. Aligned peptide-bond dipoles in α-helices create a macrodipole (Hol *et al.*,

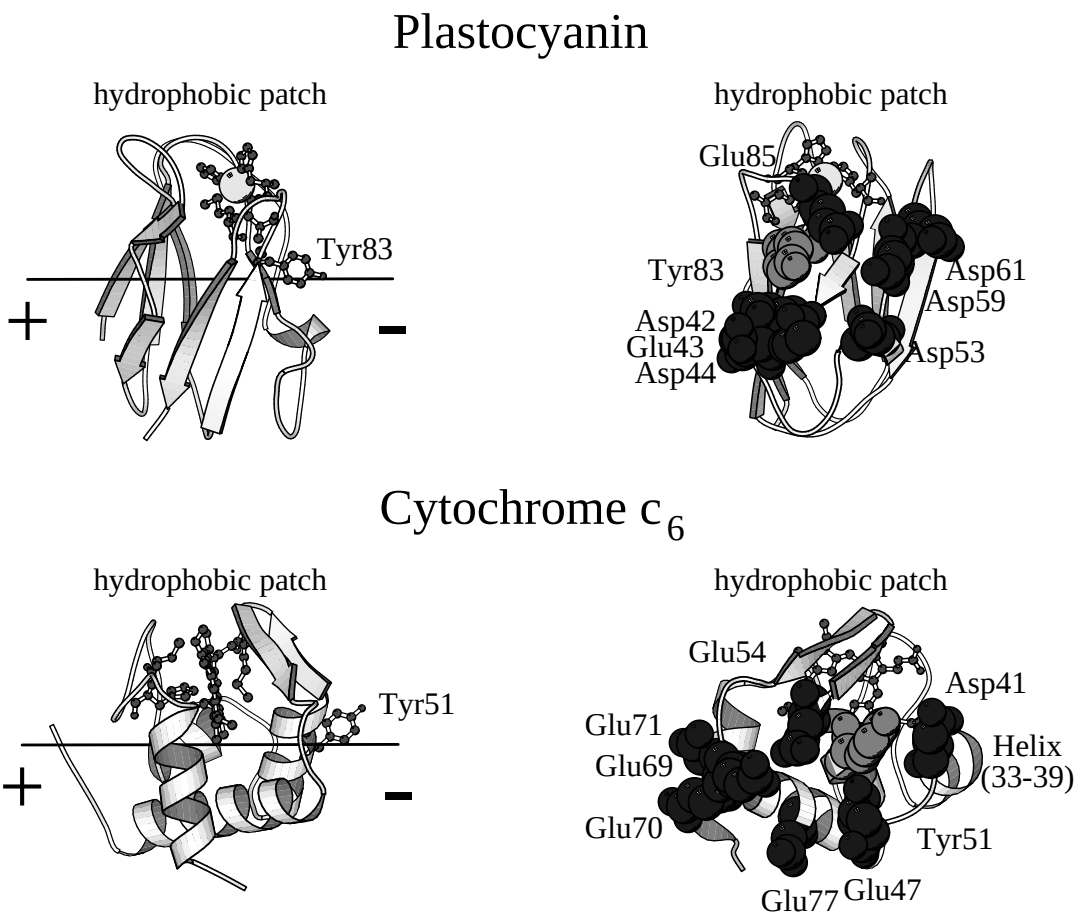

Figure 5.12: Superposition of plastocyanin and cytochrome c_6 from *Chlamydomonas reinhardtii* by alignment of their dipole moments (solid line in the right panel) and overlap of their hydrophobic patches. The magnitude of the dipole moment is not proportional to the length of the solid line. In the left panel, the ligands to the copper atoms and Tyr83 in plastocyanin and also the heme, Cys17, and Tyr51 in cytochrome c_6 are shown in balls and sticks. In the right panel, the protein molecules are rotated by 90^o around the vertical axis in the figure plane; the acidic patch points to the viewer. The residues in the acidic patches (dark grey), some of the residues in the hydrophobic patches (ball and stick), and Tyr83 in plastocyanin and Trp83 in cytochrome c_6 (light grey) are highlighted.

plastocyanin	cytochrome c_6	
	alignment of the dipoles	matching of the electrostatic fields
Asp42, Glu43, Asp44[a]	Glu69, Glu70, Glu71	Glu70, Glu71
Asp53	Glu47	Glu69
Asp59, Asp61[b]	Asp41, α-helix(33-39)	Glu54, α-helix(46-55)
Glu85	Glu54, α-helix(46-55)	Asp65

a — Three residues in the lower cluster

b — Two residues in the upper cluster

Table 5.7: Corresponding acidic residues and α-Helices in plastocyanin and cytochrome c_6 from *Chlamydomonas reinhardtii* identified in two superpositions – by overlaying centers of mass, dipole vectors, and hydrophobic patches and by optimizing the match of electrostatic potentials

protein	residue (electron pair)	distance[a] to the metal site (in Å)	squared relative electronic coupling between the residue and the metal site[b]		
			$(\prod \varepsilon_i)^2$ $\varepsilon_{arom} = 0.6$	$(\prod \varepsilon_i)^2$ $\varepsilon_{arom} = 1.0$	$(\gamma_{DL}^2 \prod \varepsilon_i)^2$ $\varepsilon_{arom} = 1.0$
plastocyanin[c]	His87 ($C_{\varepsilon 2}$-$H_{\varepsilon 2}$)	5	1.7×10^{-2}	4.7×10^{-2}	6.7×10^{-6}
	Tyr83 (C_{ζ}-O_{η})	12	4.7×10^{-6}	3.7×10^{-5}	7.7×10^{-6}
cytochrome c_6[c]	Cys17 (S_{γ} lone pair)	6	3.6×10^{-3}	7.8×10^{-2}	7.8×10^{-2}
	Trp63 ($C_{\eta 2}$-$C_{\zeta 3}$)	9	9.9×10^{-6}	5.8×10^{-2}	5.8×10^{-2}
	Tyr51 (C_{ζ}-O_{η})	15	1.2×10^{-10}	2.6×10^{-8}	2.6×10^{-8}

a – The distance is measured from the metal atom to the center of the electron pair specified in the second column

b – Values for different proteins should not be compared, because the proportionality factors in eq 3.5 and 3.6 may differ

c – from *Chlamydomonas reinhardtii*

Table 5.8: Significant amino-acid residues on the protein surface and their properties relevant to electron-transfer reactions;

1978), that can have a strong influence on the electrostatics of proteins. The dipole moment arising from the α-helix between residues 33 and 39 in cytochrome c_6 enhances the negative electrostatic potential at the position of residue 41.

The electronic coupling of Tyr51 to the heme is maintained by the sequential neighbor Gln52, which is in van der Waals contact with the heme ring. As Table 5.8 shows, however, Tyr51 is coupled weakly to the heme. The residue Gln52 is present in all known cytochrome c_6 sequences, but Tyr51 is missing in 10 sequences out of 23, and replaced by non-aromatic amino acids. Only one of the organisms lacking Tyr51 in cytochrome c_6 is an eukaryote. This sequence has been determined by Edman degradation (Okamoto *et al.*, 1987), which is sometimes unreliable. A redetermination of this sequence by a different method would be of interest. All the other cytochrome c_6 sequences lacking Tyr51 are prokaryotic proteins. These facts can be explained in two ways. Either Tyr51 is not involved in the electron-transfer reaction, or eukaryotic cytochromes c_6 do use Tyr51 in the electron-transfer reaction whereas prokaryotic cytochromes c_6 do not. The second interpretation, requiring different mechanisms for different species, seems unlikely.

5.4.2 Superposition of Plastocyanin and Cytochrome c_6 from *Chlamydomonas reinhardtii* on the Basis of their Electrostatic Potentials.

We aligned plastocyanin and cytochrome c_6 using a detailed representation of their electrostatic potentials and optimized the Hodgkin index (see Section 2.5) for the alignment (Ullmann *et al.*, 1997a). Each of one hundred optimizations started from different initial orientation. This search yielded ten different local maxima, which represent relative orientations of the proteins in which their electrostatic potentials are matched best. The two best superpositions, those with the highest Hodgkin index, differ only very little from each other; forty-one out of one hundred maximizations ended in one of these two maxima. The hydrophobic patches, for which a functional role has been suggested (Frazão *et al.*, 1995; Kerfeld *et al.*, 1995), are superimposed only in these two alignments. Only a few optimizations converged to each of the remaining eight structural alignments, which correspond to lower values of the Hodgkin indices. In some of

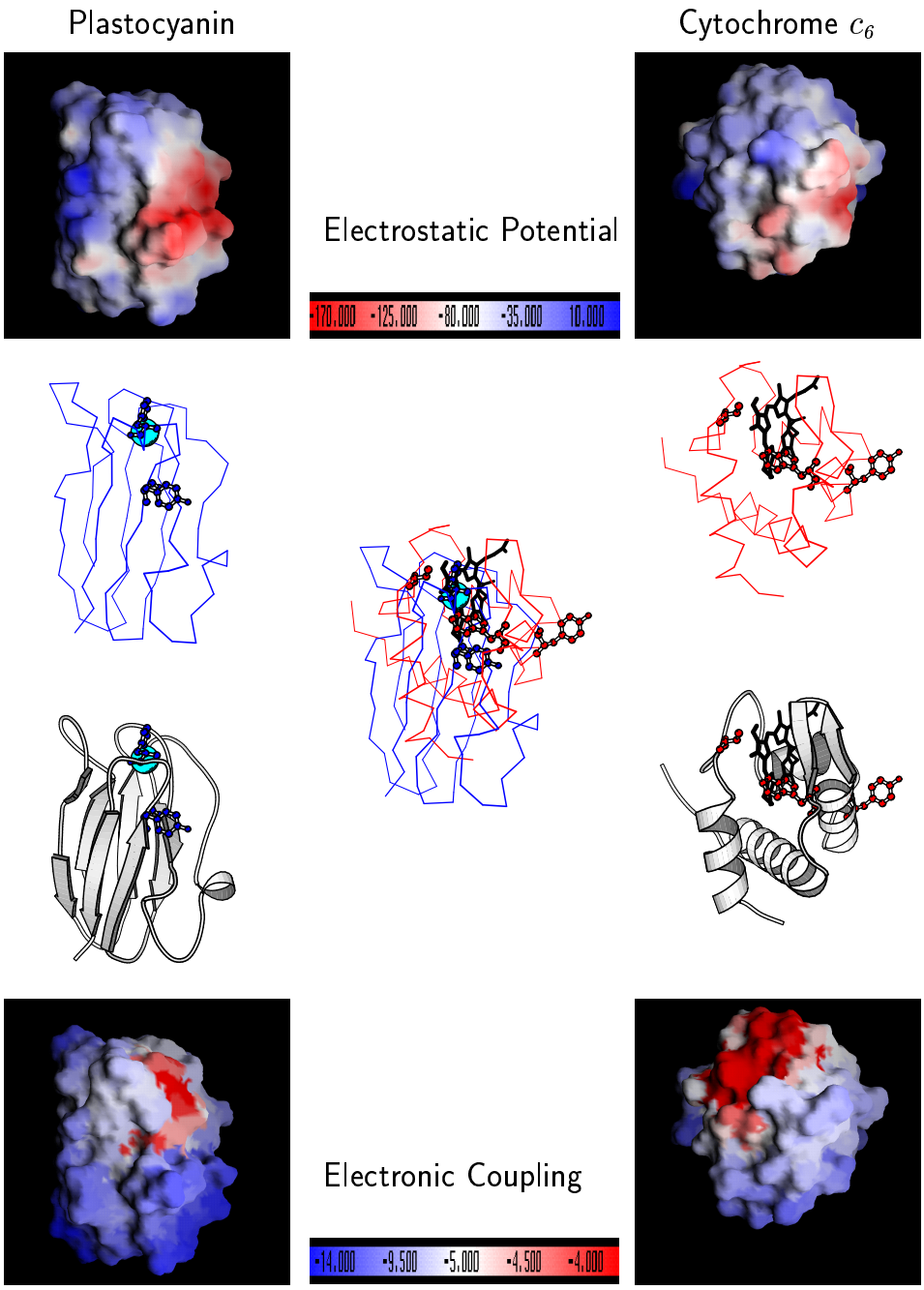

Figure 5.13: Properties of plastocyanin and cytochrome c_6 from *Chlamydomonas reinhardtii* that are relevant to the interprotein electron-transfer reaction. The superposition of the two proteins corresponding to the best match of their electrostatic potentials, i.e., the highest Hodgkin index, is shown in the middle of the figure. The separate proteins are kept in the positions so defined. Top part: electrostatic potentials calculated with the uniform dielectric constant of 4. The color is calibrated in the units of k_BT, T=298 K. Middle part: C_α-traces and secondary and tertiary structures. The copper atom, His87, and Tyr 83 in plastocyanin and also the heme, Trp63, Tyr51 and Cys17 in cytochrome c_6 are highlighted. Bottom part: Electronic coupling between surface amino-acid residues on the one hand and the iron heme site or the copper site on the other, calculated as in eq 3.6, taking into account differences in covalency of the various metal ligand bonds. The decadic logarithm of the square of the relative couplings, $\log_{10}\left(\left(\gamma_{DL}^2\prod\varepsilon_i\right)^2\right)$, is mapped onto the molecular surface of the proteins. Strongest coupling is shown in red and the weakest in dark blue.

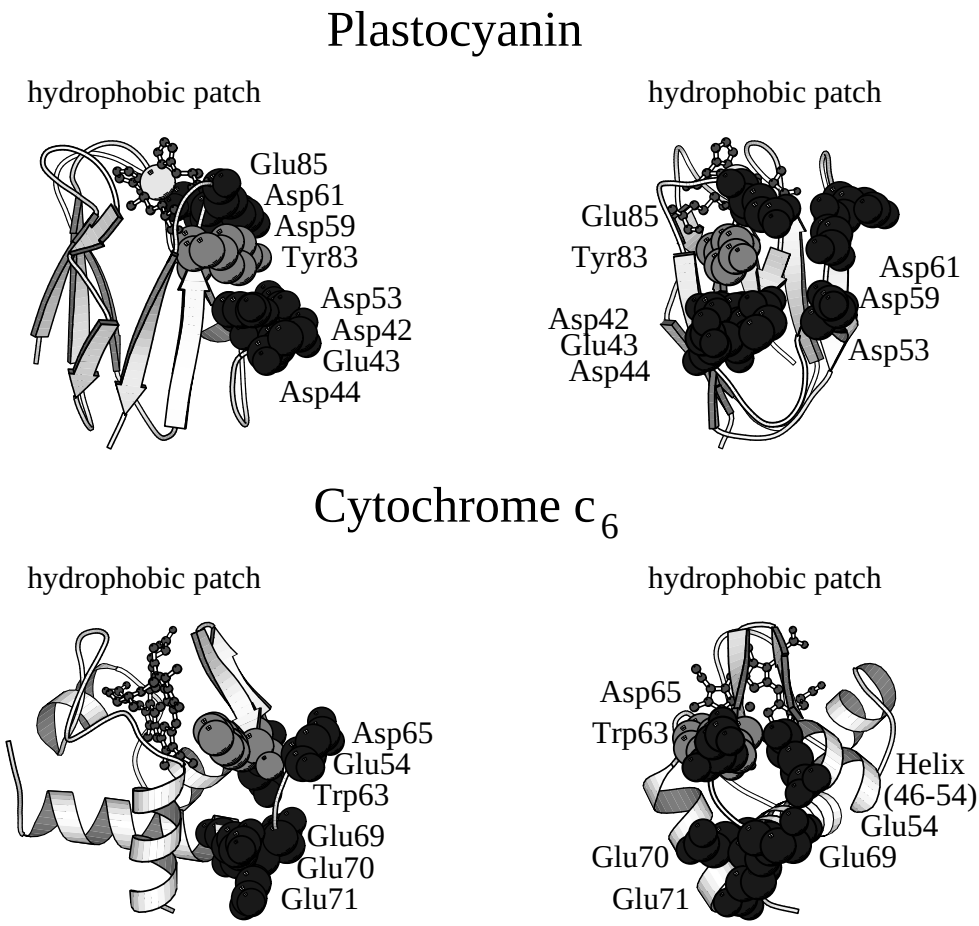

Figure 5.14: Similarity between the acidic patches on the surface of plastocyanin and cytochrome c_6 from *Chlamydomonas reinhardtii*. The two molecules in the same column adopt the positions corresponding to the best match of their electrostatic potentials, i.e., the highest Hodgkin index. On the left side of the figure, the acidic patches point to the right. On the right side of the figure, the protein molecules are rotated by 90^o around the vertical axis in the figure plane, so that the acidic patches point to the viewer. The ligands at the metal sites are shown as balls and sticks, acidic residues are dark grey, and the aromatic residues Tyr83 and Trp63 in plastocyanin and cytochrome c_6, respectively, are light grey.

these overlays, only the acidic patches overlap, while the remainders of the proteins do not. In other overlays, the hydrophobic patches are on opposite sides; these cases are uninterpretable. In the best superposition, in which the electrostatic potentials are maximally matched, functionally equivalent residues are expected to be superimposed. For that reasons, we discuss only the orientation that has the highest Hodgkin index (0.85; see Table 2.1). It is depicted in Figure 5.13.

The similarity of the values 0.85 and 0.92 in Table 2.1 indicates a high degree of similarity between the electrostatic potentials of plastocyanin and cytochrome c_6. The copper ligand His87 in plastocyanin lies only 3.5 Å away from Cys17 in cytochrome c_6, which is covalently attached heme. Both residues sit in the center of the hydrophobic patches in their respective proteins. Since this patch in plastocyanin is implicated in the electron transfer to photosystem I (Haehnel *et al.*, 1994), a similar role can be assigned to Cys17 in cytochrome c_6. A similar assignment has already been suggested (Frazão *et al.*, 1995; Kerfeld *et al.*, 1995). The residue Tyr83 in plastocyanin is implicated in the electron transfer from cytochrome f to plastocyanin (He *et al.*, 1991; Modi *et al.*, 1992b). The aromatic residue in cytochrome c_6, that sits closest

to Tyr83 in the optimal superposition is Trp63. The distance between the centers of aromatic rings of these two amino acids is only 3.5 Å. A rotation of one of the proteins by a few degrees fully superimposes Cys17 of cytochrome c_6 with the His87 of plastocyanin and also Trp63 of cytochrome c_6 with Tyr83 of plastocyanin. This latter superposition of Trp63 in cytochrome c_6 with Tyr83 in plastocyanin implies similar roles of the two aromatic residues in the electron-transfer reactions of the respective protein with cytochrome *f*. The two residues may be involved in the association with cytochrome *f* or in the subsequent electron-transfer step. An aromatic residue at position 63 can be found in all 23 known sequences of cytochrome c_6. It is tryptophane in 5 and phenylalanine in 18 sequences (see Appendix C). The replacement of one functionally important aromatic amino acid by another aromatic amino acid has been observed in several proteins. For example, Tyr83 is replaced by a phenylalanine in two algal plastocyanins (see Appendix C). The superpositions obtained from the dipole alignment suggested a function for Tyr51 in cytochrome c_6 analogous to that of Tyr83 in plastocyanin. In the superposition with the highest Hodgkin index, the aromatic ring of Tyr51 in cytochrome c_6 is 9.5 Å apart from the center of the aromatic ring of Tyr83 of plastocyanin. This long distance, a sign for non-superimposability of Tyr83 and Tyr51 can be taken as evidence against the involvement of Tyr51 in the electron-transfer reaction between cytochrome c_6 and cytochrome *f*.

Because the aromatic ring of Trp63 is in van der Waals contact with the heme, favorable coupling between them is likely. This and other couplings that may be involved in the interprotein electron-transfer reactions are given in Table 5.8. In plastocyanin, the relative couplings of His87 and of Tyr83 scaled by the expansion coefficients are comparable. The scaled relative couplings of Cys17 and of Trp63 of cytochrome c_6 are also similar (the last column in Table 5.8).

In Figure 5.14, we compare the positions of acidic residues in plastocyanin and in cytochrome c_6. Two residues are considered analogous to each other, if the distance of their acidic groups is less than 6.5 Å. These residues are listed in Table 5.4.1. Since an α-helix in cytochrome c_6 between the residues 46 and 55 ends near Glu54, the negative end of the dipole moment arising from the α-helix also contributes to the electrostatic potential at Glu54.

The pH value within the luminal space of the thylakoids is about 5. Therefore, we calculated by an established method (Bashford & Karplus, 1990) the protonation patterns for plastocyanin and cytochrome c_6 at this pH value. The superpositions found with these protonation patterns do not differ significantly from those obtained with the protonation patterns at pH 7, assuming standard pK_a values (Ullmann & Hauswald, unpublished results). Because there is no clear experimental evidence, which residues have non-standard protonation in plastocyanin or cytochrome c_6 at pH 5, we describe the results found with protonations at pH 7 assuming standard pK_a. All conclusions remain the same, when we study the proteins at the physiological pH value.

5.4.3 Possible Cation-π Interaction within Cytochrome c_6

All but two known amino-acid sequences of cytochrome c_6 contain a cationic residue (lysine or arginine) in position 66. The crystal structure (Frazão *et al.*, 1995) and the NMR spectroscopic model (Banci *et al.*, 1996) of *Monoraphidium braunii* cytochrome c_6 consistently show the spatial proximity of Arg66 and Trp63 – possibly a consequence of a cation-π interaction. Although the crystal structure of *Chlamydomonas reinhardtii* cytochrome c_6 (Kerfeld *et al.*, 1995) does not show this close proximity, a small reorientation of the side chain of Arg66 is sufficient to bring the guanidinium cation over the indole ring of Trp63, to a position required

for a cation-π interaction. Because three-dimensional structures of proteins determined by both X-ray crystallography and NMR spectroscopy are refined by classical force fields, which can normally not account for cation-π interactions (Caldwell & Kollman, 1995), minor adjustments in the positions of side chains may be justifiable. Unlike Arg88 in plastocyanin, Arg66 in cytochrome c_6 is present even in the species whose cytochrome *f* contain Lys65. In these species, Lys65 in cytochrome *f* is probably not required for an efficient electron transfer from that protein to cytochrome c_6. Another possibility would be that Lys65 in cytochrome *f* replaces Arg66 in cytochrome c_6 in the cation-π system after the formation of the protein complex. In the two species, in which the cation at position 66 is missing, the cation-π system can presumably form between Lys65 in cytochrome *f* and Trp63 in cytochrome c_6.

We recognize a possibility of a cation-π interaction between Arg66 and Trp63 within cytochrome c_6. The electron-transfer reaction between cytochrome *f* and cytochrome c_6, as well as that between cytochrome *f* and plastocyanin, discussed above, may conceivably occur in two steps with an anion-radical as a transient intermediate.

5.5 Discussion of a NMR Study on the Interaction of Plastocyanin and Cytochrome *f*

After we finished and published our study on the association of French bean plastocyanin and turnip cytochrome *f* (Ullmann *et al.*, 1997b), Ubbink *et al.*, 1998 published a paper about NMR investigations on the complex of spinach plastocyanin and turnip cytochrome *f*. Using informations from diamagnetic and paramagnetic NMR, and additional electrostatic restraints, a structural model for the complex was proposed. Ubbink *et al.*, 1998 used our structure of the plastocyanin-cytochrome *f* complex for backcalculating the pseudocontact shift and for determining restraints violations. According to their calculations, our structure has an energy that is below the threshold of the rigid body molecular dynamics simulation done by Ubbink *et al.*, 1998 and would therefore have been considered as low energy structure by these authors. Several violations of NMR constraints may arise from not fully converged simulations and from slightly wrong orientations. Besides we used French bean plastocyanin in our simulation, while spinach plastocyanin was used in the experiment, which might be a further reason for the minor deviations. Based on the NMR experiment by Ubbink *et al.*, 1998, the rearrangement model which was first proposed by Qin & Kostić, 1993 and for which we offered a structural model (Ullmann *et al.*, 1997b), seems to be the correct interpretation of the experimental findings discussed in the previous sections.

If the model proposed by Ubbink *et al.*, 1998 is correct, the electron transfer via the hydrophobic path of plastocyanin is more likely than an electron transfer via the acidic patch. An electron transfer via the hydrophobic path raises, however, the question about the functional significance of highly-conserved Tyr83 of plastocyanin. A function in stabilizing the protein structure can be ruled out since the mutants of plastocyanin exist in which Tyr83 is replaced by leucine and other non-aromatic amino acids. Also a function in the electron transfer to photosystem I is unlikely as recent experiments showed (Haehnel *et al.*, 1994). We proposed the involvement of Tyr83 in association or in association and in electron transfer. Namely, we suggested that Tyr83 forms a cation-π complex with Lys65 of cytochrome *f*. The idea that this cation-π complex is involved in electron transfer is not supported by the NMR experiment of Ubbink *et al.*, 1998. However, the involvement of the cation-π complex in association is still possible and I will discuss this possibility below. Furthermore, the presence of intramolecular

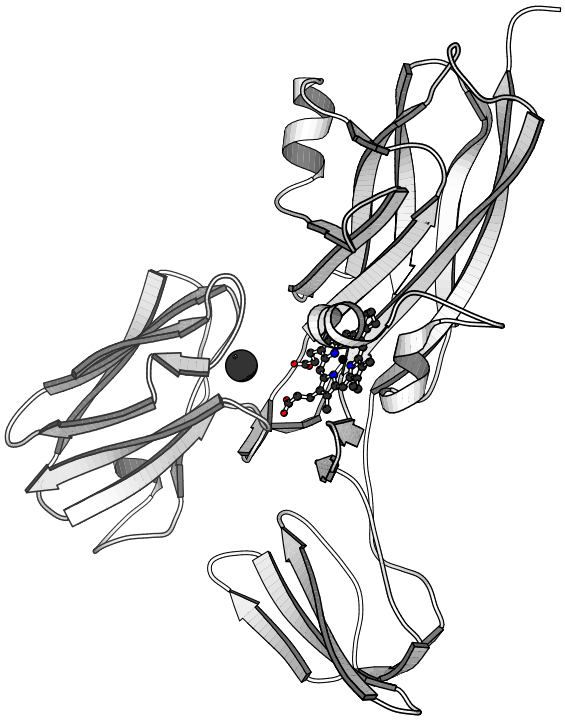

Figure 5.15: Structure of the complex formed by plastocyanin and cytochrome *f* modeled on the basis of NMR measurements. The structure determined by NMR investigation principally resembles our modeled complex structure D (see Section 5.3).

cation-π complexes in plastocyanins of organisms that lack Lys65 in cytochrome *f* (Ullmann *et al.*, 1997a) is a hint that a cation-π complex may have a special function in plastocyanin-cytochrome *f* complexes that goes beyond mediating protein association.

Cytochrome *f* shows a ridge of cationic residues at the docking interface to plastocyanin formed by Lys65, Lys181, Arg184, Lys185, and Lys187. The complex structure proposed by Ubbink *et al.*, 1998 includes Tyr160 in the interface, i. e., plastocyanin binds close to the ridge; Tyr83 and Lys65 are far apart from each other. In our complex D, plastocyanin binds more or less directly at the ridge of cytochrome *f*; Tyr83 and Lys65 are closer to each other but are still not in direct contact. A binding of plastocyanin at the site of the ridge opposite to that proposed by Ubbink *et al.*, 1998 would enable the interaction of Tyr83 and Lys65. In this binding mode, the hydrophobic patch of plastocyanin binds close to the heme site of cytochrome *f*. This close proximity may also explain the pseudocontact shift observed by NMR. Since the constraints used in the rigid body refinement beside the pseudocontact constraints seem to be rather unspecific, this slightly different orientation may agree with experiments as well. The binding of plastocyanin to cytochrome *f* may then proceed in two steps. First, the binding occurs in an orientation similar to the orientation in complex D. The cation-π complex may form during this initial binding. Crosslinking by carbodiimides may also take place at this step. Second, plastocyanin diffuses on the surface of cytochrome *f* to its final, electron-transfer active orientation. The cation-π complex between Tyr83 and Lys65 would remain intact during the reorientation and probably tighten the complex. In the final orientation, the cation-π complex may lie close to the chain of buried water molecules found by X-ray crystallography (Martinez *et al.*, 1996). This internal water chain is discussed to be involved in proton transfer reaction. Binding of a cation to a phenol ring may raise the redox potential of the phenol ring as discussed above.

But it may also lower the proton affinity of the hydroxyl group of the phenol ring. A lower pK_a of the hydroxyl group of the phenol ring of tyrosine makes Tyr83 to a possible participant in a proton transfer chain. The proximity to the internal water chain of cytochrome *f* further supports this suggestion. Therefore, the function of the proposed cation-π complex may be the involvement in a proton transfer. A somewhat different orientation in complex D may also change the energy of complex D and the energy ranking of the complexes may change in favor of complex D. The reason why we were not able to find this different binding mode in the Monte Carlo and molecular dynamics simulation may be the use of classical force fields, which do not properly account for cation-π interactions. Also the internal cation-π complex between Trp63 and Arg66 in cytochrome c_6 may be able to participate in a proton transfer reaction. In some cases, phenylalanine replaces Trp63. Since phenylalanine has no hydroxyl group, it may not participate in a proton transfer reaction. Cation-π complexes that involve arginine residues can show a π-π interaction in addition to the cation-π interaction (Ma & Dougherty, 1997). The π-π interaction between arginine and phenylalanine may change the pK_a of arginine, thus the arginine could participate in the proton transfer chain. The involvement of Tyr83 in binding and in proton transfer would assign a function to this residue. Furthermore, would also explain why an intramolecular cation-π complex is form in plastocyanin of organisms that lack Lys65 in cytochrome *f*.

The interpretations proposed here base on investigations on protein structures and sequences. Nevertheless, they are to some extent speculative and need experimental proof and further theoretical investigations. The influence of cation-π binding on pK_a values may be investigated on model compounds. These studies can be done experimentally as well as theoretically. Theoretical investigations of the involvement of cation-π binding in protein association is a challenge for the future since the inclusion of cation-π binding contributions in molecular dynamics or Monte Carlo calculations is only in its infancy (Caldwell & Kollman, 1995).

5.6 Comparison of the Isofunctional Electron-Carrier Proteins Ferredoxin and Flavodoxin

The Fe_2S_2 protein ferredoxin (Fd) serves as a soluble electron carrier in the light phase of photosynthesis. It transports electrons between photosystem I (PSI) and ferredoxin-$NADP^+$ reductase (FNR) in the stroma of chloroplasts and in cyanobacteria (Knaff & Hirasawa, 1991). FNR uses the electrons received from two Fd's to reduce $NADP^+$, which is required to synthesize carbohydrates in the dark phase of photosynthesis. Ferredoxin is also involved in the cyclic electron transport, which leads to an increase of the pH gradient between stroma and thylakoid space and thus to an increased production of ATP (Bendall & Manasse, 1995). Besides, Fd delivers electrons to other proteins such as for instance nitrite reductase, sulfate reductase, glutamate synthase, and ferredoxin-thioredoxin reductase (Knaff & Hirasawa, 1991). Therefore Fd plays a central role for many redox reactions in chloroplast and cyanobacteria as well as in the regulation of photosynthesis. Under conditions of iron deficiency, the flavin-containing protein flavodoxin (Fld) can replace Fd in some reactions in most cyanobacteria and some eukaryotic algae. The electron transfer reactions of Fd with its reaction partners have been investigated extensively (for review see Knaff & Hirasawa, 1991). Much less studies were done on the electron-transfer reactions of Fld with its reaction partners (Navarro *et al.*, 1995 and references cited therein).

The redox potential of Fd from *Anabaena* PCC 7120 for the redox couple $Fe^{III}Fe^{II}/Fe^{III}Fe^{III}$

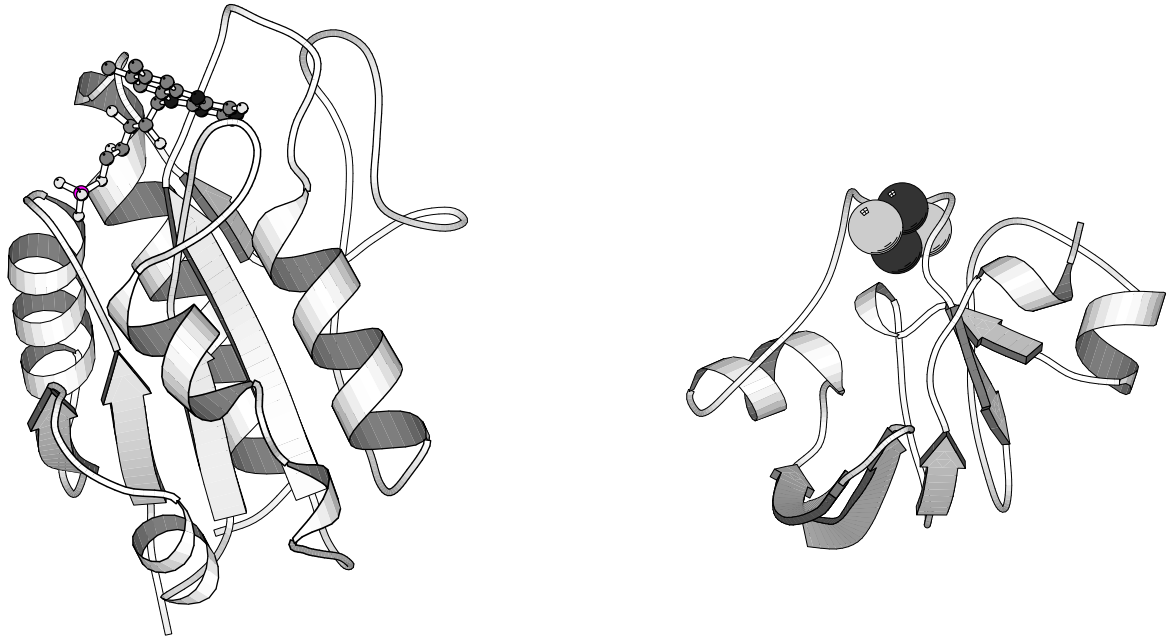

Figure 5.16: Structures of Ferredoxin and Flavodoxin. Although both proteins differ in structure and size, they can perform the same physiological function.

is -430 mV (Hurley *et al.*, 1993b). The fully-oxidized form of native Fd has never been detected (Im *et al.*, 1998) and is therefore believed to play no physiological role. The redox potential difference between the fully-reduced from and the semi-reduced from of Fld is -436 mV, that between the semi-reduced from to the fully oxidized form is -212 mV at pH 7.0 (Pueyo *et al.*, 1991). With regard to the redox potential, it is believed that Fld alternates between the semi- and fully-reduced state in the photosynthetic electron-transfer chain, although this has not been shown rigorously (Mühlenhoff & Sétif, 1996). The flavin in Fld is sandwiched between Trp57 and Tyr94. The π-stacking interaction between these two aromatic rings of the amino acid side-chains and the aromatic ring of the flavin causes a strong binding of the cofactor and also influences the redox potential of flavin (Lostao *et al.*, 1997; Breinlinger & Rotello, 1997).

The structures of various plant-type Fd's (Smith *et al.*, 1983; Tsukihara *et al.*, 1990; Rypniewski *et al.*, 1991; Fukuyama *et al.*, 1995; Baumann *et al.*, 1996; Hatanaka *et al.*, 1997) and Fld's (Fukuyama *et al.*, 1990; Rao *et al.*, 1993) have been determined by X-Ray crystallography and by NMR spectroscopy. For the cyanobacteria *Anabaena* PCC 7120, the structures of Fd (Rypniewski *et al.*, 1991) and Fld (Rao *et al.*, 1993) are known. There are only minor structural variations among different plant-type Fd's and among cyanobacterial and algal Fld's. The structures of Fd and Fld from the same species differ, however, completely. In fact, they differ not only in structure but also in size (Figure 5.16). Fd is with about 100 amino acids smaller than the Fld with about 170 amino acids. Fd and Fld share neither a common secondary structure nor a common tertiary fold.

Together with Markus Hauswald, Axel Jensen, and Ernst Walter Knapp, I superimposed Fd and Fld by optimizing the overlap of their electrostatic potentials (Ullmann *et al.*, 1998a). The obtained superpositions are correlated with structural and other experimental data that are

available for the interaction of Fd and Fld with PSI and with FNR. Before discussing the results of the structural alignment of Fd and Fld, I give a brief overview of experimental data for the interactions of these proteins with its physiological partners.

5.6.1 Experimental Studies on the Interaction of Ferredoxin and Flavodoxin with Photosystem I

Fd and Fld can be chemically-crosslinked to PSI (Zanetti & Merati, 1987; Wynn *et al.*, 1989). Since the electron-transfer rates are similar to those of the electrostatic complexes, the crosslinked complexes are likely to resemble electrostatic complexes (Mühlenhoff *et al.*, 1996a; Lelong *et al.*, 1996). The crosslinking takes place between Glu93 of Fd from *Synechocystis* (Glu95 in Fd from *Anabaena* PCC 7120) and Lys106 of subunit PsaD of PSI (Lelong *et al.*, 1994). Surprisingly, the mutations of Lys106 in subunit PsaD show only small effects on the electron-transfer reaction (Hanley *et al.*, 1996; Chitnis *et al.*, 1996). The mutation Lys106Cys does, however, affect the electron transfer reaction, indicating that this cysteine may be negatively charged in the PSI (Hanley *et al.*, 1996; Chitnis *et al.*, 1996). Mutation studies on Fd from *Anabaena* PCC 7120 revealed that Glu31, Arg42, Thr48, Asp67, Asp68, Asp69, Glu94, and Glu95 influence the bimolecular electron transfer from PSI to Fd and are thus involved either in the binding reaction or in the electron transfer (Navarro *et al.*, 1995). Recent mutation studies indicate the involvement of Lys35 in subunit PsaC of PSI in the docking and crosslinking of ferredoxin to PSI (Fischer *et al.*, 1998). The residues Trp57, Glu61, Glu67, Asp126, and Glu145 of Fld influence the electron transfer reaction with PSI (Navarro *et al.*, 1995).

Further investigations showed that the binding of Fd and Fld involves the subunits PsaC, PsaD, and PsaE of PSI and a membrane-embedded 15-kDa subunit, probably subunit PsaF (Rousseau *et al.*, 1993; Sonoike *et al.*, 1993; Mühlenhoff *et al.*, 1996b; Fischer *et al.*, 1997; Schubert *et al.*, 1997; Fischer *et al.*, 1998). A biphasic kinetic for the electron transfer from PSI to Fd lead to the suggestion that there are two separate Fd-binding sites on PSI (Sétif & Bottin, 1994; Sétif & Bottin, 1995). Covalent complexes between Fld and PSI are however not able to reduce soluble Fd or Fld, which indicates that there is only a single Fd-binding site (Mühlenhoff *et al.*, 1996b; Mühlenhoff *et al.*, 1996a). The crosslinked complexes have been investigated by electron microscopy (Mühlenhoff *et al.*, 1996a; Lelong *et al.*, 1996). It was found that Fd and Fld dock at the same binding site and that the electron densities of both proteins in the microscopic pictures overlap almost completely. However, the electron densities are not concentric. Non-concentric electron densities may indicate that both proteins try to arrange their prosthetic groups as close as possible to the terminal electron acceptor in PSI (Lelong *et al.*, 1996). This interpretation is in agreement with a more peripheral localization of Fld on PSI relative to Fd.

Recently, a structural model of PSI from the cyanobacteria *Synechococcus elongatus* that is based on 4 Å resolution X-ray data has been published (Krauss *et al.*, 1996; Schubert *et al.*, 1997). On the basis of the 6 Å electron density map of PSI (Krauss *et al.*, 1993), it was proposed that Fd binds to a cavity formed by stromal subunits (Fromme *et al.*, 1994). The subsequent electron microscopic analyses (Mühlenhoff *et al.*, 1996a; Lelong *et al.*, 1996) support this model. Presumably, two one-turn α-helices of PsaC, surface regions of PsaD and PsaE and the α-helix E (either PsaA or PsaB) constitute the Fd binding site (Schubert *et al.*, 1997).

5.6.2 Experimental Studies on the Interaction of Ferredoxin and Flavodoxin with Ferredoxin-NADP$^+$ Reductase

The interaction between Fd and FNR has been investigated extensively (Chan *et al.*, 1983; Vieira *et al.*, 1986; Zanetti *et al.*, 1988; Sancho *et al.*, 1990; Walker *et al.*, 1991; Pueyo *et al.*, 1992; De Pascalis *et al.*, 1993; Jeresarov *et al.*, 1993; Hurley *et al.*, 1993b; Hurley *et al.*, 1993a; Hurley *et al.*, 1994; Aliverti *et al.*, 1994; Aliverti *et al.*, 1994; Navarro *et al.*, 1995; Hurley *et al.*, 1996b; Hurley *et al.*, 1996a; Piubelli *et al.*, 1996; Aliverti *et al.*, 1997; Hurley *et al.*, 1997; Medina *et al.*, 1998). Considerably less investigation exist on the interaction of Fld and FNR (Walker *et al.*, 1990; Pueyo *et al.*, 1991; Pueyo & Gomez-Moreno, 1991; Medina *et al.*, 1992a; Medina *et al.*, 1992b; Navarro *et al.*, 1995). I briefly review the available experimental data on the interaction of these proteins.

The proteins Fd and FNR can be chemical crosslinked mediated by carbodiimides. The residues Glu92 of spinach Fd (Glu94 in Fd from *Anabaena* PCC 7120) and the residue Lys85 or Lys86 of spinach FNR (Lys69 or Lys72) were identified as crosslinking sites (Zanetti *et al.*, 1988). However, Fd mutants and FNR mutants, in which these residues are replaced by crosslink-inactive uncharged amino acids, can still be chemically crosslinked, but the rate of crosslinking decreases (Aliverti *et al.*, 1994; Piubelli *et al.*, 1996; Aliverti *et al.*, 1997). Furthermore, these mutants show less efficient electron-transfer reactions in the electrostatic complex, indicating that the mutated residues are involved in the electron-transfer reaction or, more likely, in the recognition of the reaction partners (Aliverti *et al.*, 1994; Piubelli *et al.*, 1996; Aliverti *et al.*, 1997). Differential chemical modification studies on spinach Fd suggest that Asp26 (Asp28 in Fd from *Anabaena* PCC 7120), Glu29 (Glu31), Glu30 (Glu32), Asp34 (Asp36), Asp65 (Asp67), and Asp66 (Asp68) are buried at the interface, since these residues are protected against chemical modification in the associated complex (De Pascalis *et al.*, 1993). The same approach revealed that in spinach FNR, Lys18 (not present in FNR from *Anabaena* PCC 7119), Lys33 (Arg16), Lys35 (not present), and Lys153 (Lys138) are buried in the interface of the protein complex (Jeresarov *et al.*, 1993). Also arginines are involved in the association of Fd and FNR (Sancho *et al.*, 1990). Concluding from differential chemical modification studies and from a modeling study it was proposed that Asp26 (Asp28), Glu29 (Glu31), Glu30 (Glu32), and Asp34 (Asp36) of spinach Fd interact with Lys304 (Lys293) and Lys305 (Lys294) of spinach FNR and that Asp65 (Asp67) and Asp66 (Asp68) of spinach Fd interact with Lys33 (Arg16), Lys35 (not present), Lys91 (Lys75) and Arg93 (Arg77) of spinach FNR (De Pascalis *et al.*, 1993). Earlier studies also imply that these residues of Fd participate in the association (Vieira *et al.*, 1986). The ionic strength dependence of the electron-transfer reaction makes it likely that besides electrostatic interactions also hydrophobic interactions play an important role in the complex formation (Walker *et al.*, 1991; Hurley *et al.*, 1996a). The residues Asp67, Asp68, Asp69, Thr48, and Arg42 also affect the second-order rate constant of the electron-transfer reaction (Hurley *et al.*, 1993b; Hurley *et al.*, 1996b). The mutants Asp62Lys, Asp68Lys, Gln70Lys, Glu94Asp, Glu95Lys, Phe65Tyr, and Ser47Thr modulate the second order rate constants of the electron-transfer reactions (Hurley *et al.*, 1997). In addition to the mutants Glu94Lys, Phe65Ile, and Phe65Ala (Hurley *et al.*, 1993a; Hurley *et al.*, 1993b), the mutants Glu94Gln and Ser47Ala are virtually not able to transfer electrons to FNR (Hurley *et al.*, 1997). It was shown that Fd requires an aromatic amino acid at position 65 for an efficient electron transfer (Hurley *et al.*, 1993a). The amino acid Glu301 of FNR seems to be involved in the catalytic mechanism of FNR, probably in the protonation of the reduced form of NADP$^+$ (Medina *et al.*, 1998).

Also Fld and FNR from *Anabaena* PCC 7119 can be also crosslinked in 1:1 stoichiometry

Ferredoxin	Flavodoxin	
	Alignment 1	Alignment 2
Glu19	—	**Asp123**
Asp22, Asp23, Glu24	Glu72, Asp43, Glu40	**Asp126**, **Asp129**
Glu94, Glu95	Asp90, Asp96, Asp129	Asp35, Glu16
Asp28, **Glu31**, Glu32	Asp65, **Glu67**	**Asp144, Glu145, Asp146**
Asp67, Asp68, Asp69, Glu72	**Glu145**, Asp150, Asp153, Asp154	**Glu67**, Glu72
C-Terminus	**Glu126**	–
Arg42	–	Lys14
Helix 68-73	Helix 149-166	–

Table 5.9: Putatively corresponding residues in ferredoxin and flavodoxin from *Anabaena* PCC 7120 identified in two superpositions obtained by optimizing the match of electrostatic potentials. Residues for which an involvement in the association reaction was implied experimentally are marked in bold face.

(Pueyo & Gomez-Moreno, 1991). Chemical modification studies on Fld from *Anabaena* PCC 7119 suggest that the residues Asp123, Asp126, Asp129, Asp144, Asp145, and Asp146 of Fld interact with FNR (Medina *et al.*, 1992a). Also arginine residues of Fld are involved in the interaction with FNR (Medina *et al.*, 1992b). Mutation studies show the involvement of residues Asp126 and Glu67 in the association reaction (Navarro *et al.*, 1995). The redox potentials of Fld and of FNR are affected by the association (Pueyo *et al.*, 1991).

5.6.3 Alignment of the Electrostatic Potentials of Ferredoxin and Flavodoxin from *Anabaena* PCC 7120

The electrostatic potentials of Fd and Fld were superimposed by maximizing their Hodgkin-Index (eq 2.44) using a detailed representation of their electrostatic potentials. Each of 100 optimizations started from a different initial orientation. The search yielded four different superpositions. All of them have Hodgkin Index values greater than 0.9 indicating a high degree of similarity. Two of the superpositions overlap only partially and are thus not interpretable. Namely, the acidic regions of Fd and Fld, i. e., the putative docking region, overlap while the remainder of the proteins does not. In the remaining two superpositions, Fd and Fld overlap almost completely. Both proteins are, however, not concentric in the superpositions, which is in agreement with observations from the electron microscopy on crosslinked Fd-PSI and Fld-PSI complexes (Mühlenhoff *et al.*, 1996a; Lelong *et al.*, 1996).

The values of the Hodgkin index for the first and for the second alignment, respectively, are 0.94 and 0.92. The high values indicate a high degree of similarity of the two proteins. Out of 100 optimizations, 31 and 30 minimizations ended at the first and at the second ranked alignment, respectively. The two superpositions of Fd and Fld, their electrostatic potentials, and their relative electronic coupling are shown in Figure 5.17. A rotation of about 180^{o} around an axis in the plane of Figure 5.17 that goes from the bottom to the top of the sheet relates the two superpositions of Fd and Fld to each other. The residues in these two proteins that may have a similar function in the recognition of the reaction partners are listed in Table 5.9 and depicted in Figure 5.18. Two residues are considered to be isofunctional, if the distance of their acidic groups in the superposition is less than 6.5 Å. This distance seems large at the first glance but can easily be bridged by an reorientation of the amino acid sidechains. Also the redox centers of

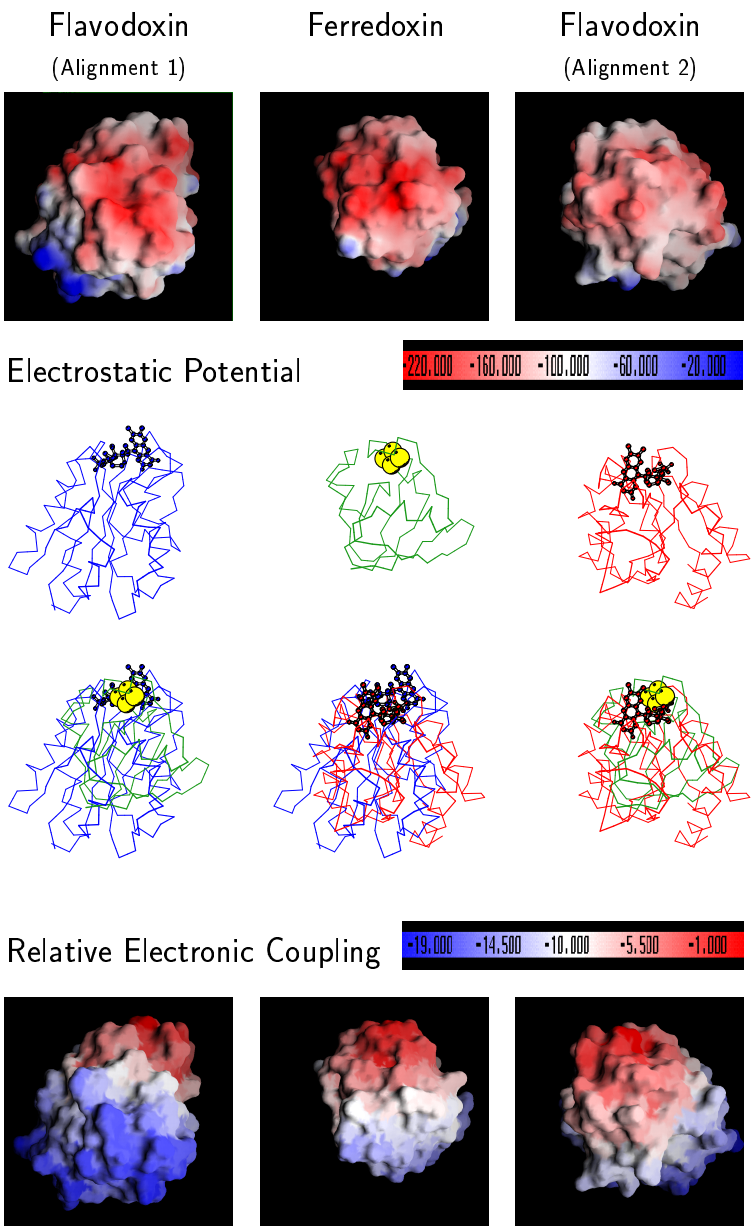

Figure 5.17: Properties of ferredoxin and flavodoxin from *Anabaena* PCC 7210 that are relevant to the interprotein electron-transfer reaction. The superposition of the two proteins corresponding to the best match of their electrostatic potentials, i.e., the highest Hodgkin index, is shown in the middle of the figure. The separate proteins are kept in the positions so defined. First row: electrostatic potentials calculated with the uniform dielectric constant of 4. The color is calibrated in the units of k_BT, T=298 K. Second row: C_α-traces of ferredoxin and flavodoxin. The redox centers are high-lighted. Third row: Superposition of ferredoxin and flavodoxin. In the left and right picture the first and the second alignment are shown, respectively. Ferredoxin is show in the same orientation in both alignments. In the middle picture, the orientation of flavodoxin for the two alignments is shown. Ferredoxin is omitted for the sake of clarity. Fourth row: Electronic coupling between surface amino-acid residues on the one hand and the iron heme site or the copper site on the other, calculated as in eq 3.6, taking into account differences in covalency of the various metal ligand bonds. The decadic logarithm of the square of the relative couplings, $\log_{10}\left(\left(\gamma_{DL}^2\prod\varepsilon_i\right)^2\right)$, is mapped onto the molecular surface of the proteins. Strongest coupling is shown in red and the weakest in dark blue.

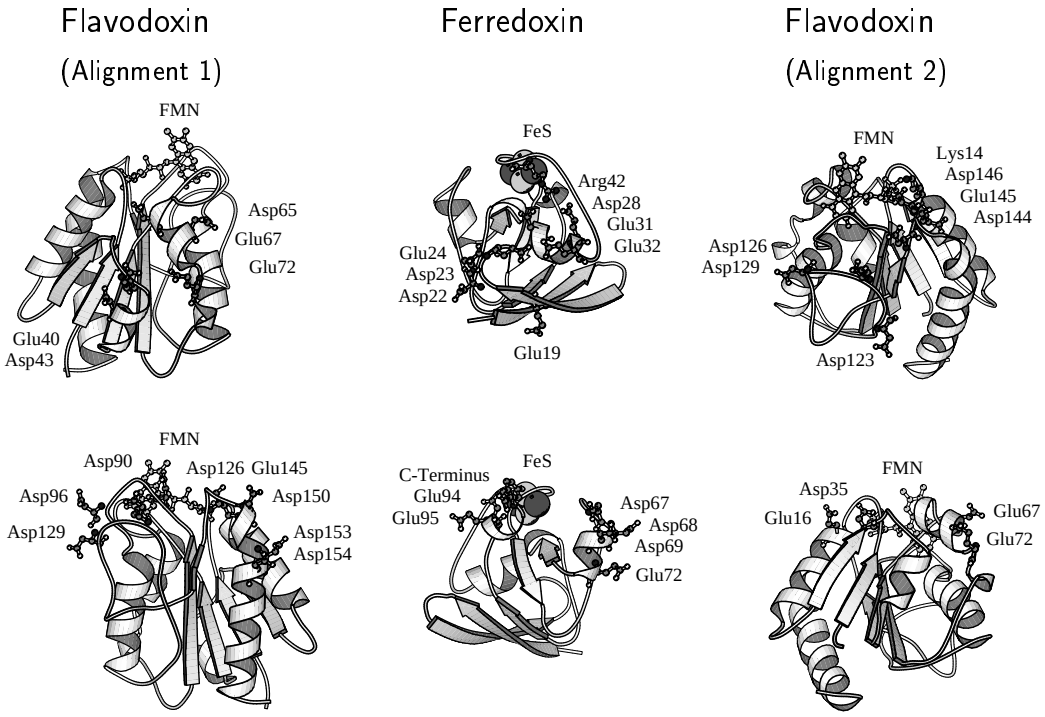

Figure 5.18: Similarity between the the acidic patches of flavodoxin and ferredoxin. The molecules in the second row are rotated by 180^o with respect to the molecules in the upper row. Residues that are putatively important are high-lighted.

Fd and Fld overlap in both superpositions. Namely, the iron-sulfur center is at the same position as residue Trp57, which makes a π-stacking interaction with the flavin of Fld.

The first alignment shows an interesting feature. The α-helix (68-73) in Fd superimposes with the α-helix (149-166) in Fld. Both α-helices have the same orientation. The negative pole of the dipole moment of the α-helices points, however, away from the putative docking site and does thus not contribute to the negative electrostatic potential at the docking site. Acidic residues that are part the α-helices are probably involved in the association of Fd and of Fld to FNR. Possibly, the shape of the α-helix is important for the association rather than its contribution to the electrostatic potential at the binding site.

Arg42 of Fd is a conserved, positively-charged residue within a negatively-charged region. This residues may influence the redox properties of the iron-sulfur cluster. But it may also provide specific recognition of the reaction partners. Interestingly, Arg42 superimposes with Lys14 of Fld in the second superposition. Lys14 of Fld is the only positively-charged residue within a negatively-charged region. In other sequences of Fld, this lysine is replaced by a asparagine, which can also work as a hydrogen bond donor. Possibly, a hydrogen-bond donor is required at this position to provide specific recognition of Fd and Fld by the redox partners.